Marine and Petroleum Geology xxx (xxxx) 105230

Contents lists available at ScienceDirect

Marine and Petroleum Geology

journal homepage: www.elsevier.com/locate/marpetgeo

# Morphostructure, emplacement and duration of the Abrolhos Magmatic Province: A geophysical analysis of the largest post-breakup magmatism of the South-Eastern Brazilian margin

Natasha Stanton [a, *], Andres Gordon PhD [a], Cassia Cardozo MsC [a], Nick Kusznir PhD [c]

[a] University of Rio de Janeiro State, Brazil
[b] AG-GEO Consulting, UK
[c] University of Liverpool, UK

ARTICLE INFO

*Keywords:*
Abrolhos magmatic province
Brazilian rifted margin
Post-breakup magmatism
Volcanic bodies
Hotspot
Mantle plume
South Atlantic

ABSTRACT

The Abrolhos Magmatic Province (AMP), located in the Ocean Continent Transition (OCT) of the Brazilian South Atlantic rifted margin, is spatially extensive covering an area larger than 63,000 km$^2$ and was emplaced in the Early Cenozoic, approximately 40 Ma after rifted margin formation in Early Cretaceous. The explanation for the origin of the AMP is that it forms part of a hotspot track that initiated at ~85 Ma in the Poxoréu region, an igneous province located ~1500 km to the west of the AMP, within Brazilian continental lithosphere and is presently located under Trindade and Martin Vaz Islands at the Vitoria-Trindade seamount chain (VTC). The aim of this work is to investigate the morphostructure, duration and spatial distribution of the AMP, exploring its significance for the margin evolution and possible origins. The magnetic, reflexion seismic and well data analysis show that the AMP consists of an assembly of large volcanic edifices formed during the Paleogene, each with individual diameters in excess of 50 km, sizes varying from 280 to 2100 km$^2$, and formed by multiple volcanic events. The igneous bodies are mainly buried at different depths (from ~2 Km to 8 km below seafloor), while some emerge to form the Abrolhos Archipelago. The spatial arrangement of the igneous edifices of the AMP suggest that in its central part are the main feeders for the outer and shallower bodies at the borders which have a radial distribution. Their distribution seems to partially follow preexisting structural trends like Precambrian and Mesozoic weakness zones, represented by the onshore Paramirin Aulacogen, the Araçuaí and Ribeira belts, and the offshore rifting structures. These observations suggest an influence of lithosphere inheritance on the emplacement of the AMP. The tectono-stratigraphic architecture indicate margin uplift at Early Cenozoic related to the emplacement of the AMP, creating an elevated area. Mapped hydrothermal vents indicate AMP magmatic activity continued into the Neogene, and connect Abrolhos volcanism with that in the VTC located 650 km to the east. This and reported low S-wave velocity from tomographic model and anomalous dynamic topography suggest a distinct mantle thermal structure under the AMC and VTC. However, the spatial extent and duration of the AMP are inconsistent with a fixed hotspot mechanism and linear trail.

## 1. Introduction

Most rifted margins are affected by magmatic events during the extensional process (White and Mckenzie, 1989; Franke, 2013). After continental breakup, their magmatic activity ceases or diminishes and passive continental margins subside thermally (White and McKenzie, 1989). Exceptions for this rule are, for example, the "passive-aggressive margin" of the North Atlantic (Mazza et al., 2017), the Newfoundland margin and South China Sea margin (Tucholke and Sibuet, 2007; Sun et al., 2020) which registered tectonic and magmatic rejuvenations.

The formation of the South Atlantic rifted margins started in the Early Cretaceous (Rabinowitz and LaBreque, 1979; Chang et al., 1992). The rift propagated from south to north, generating a variety of crustal structures with differing magmatic additions (Blaich et al., 2011). In the central segment of the South Atlantic (Moulin et al., 2010), the volume of the syn-rift magmatism at the Brazilian margin decreases from southern Santos basin to the north (Chang et al., 1992; Blaich et al., 2011), with Espirito Santo and Mucuri basins characterized by only localized volcanism (França et al., 2007). An Aptian salt basin occurs in this segment and breakup is estimated around 112 Ma (Torsvik et al.,

* Corresponding author.
*E-mail addresses:* natasha.stanton@uerj.br (N. Stanton), acgordon@ymail.com (A. Gordon), njkgeos@outlook.com (N. Kusznir).

https://doi.org/10.1016/j.marpetgeo.2021.105230
Received 13 September 2020; Received in revised form 7 July 2021; Accepted 9 July 2021
0264-8172/

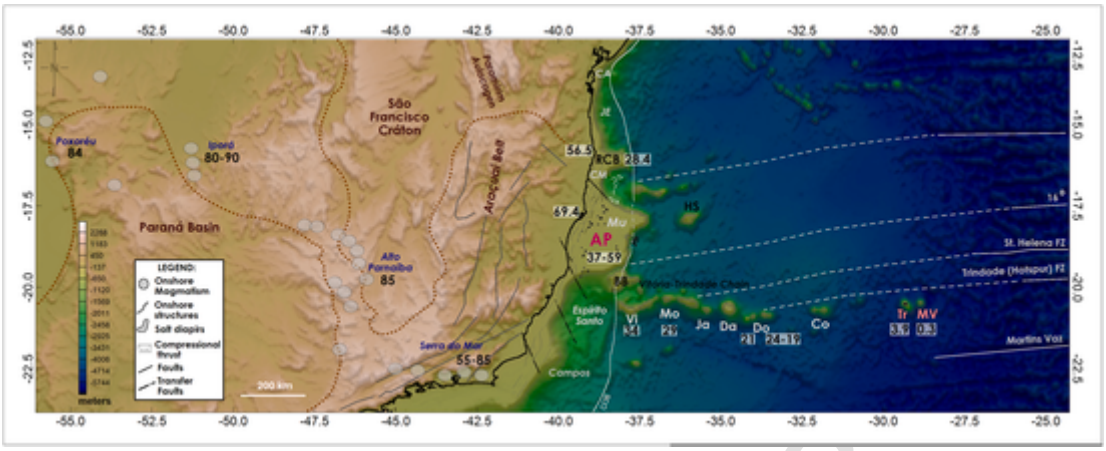


**Fig. 1.** Bathymetry/topography map of the study area, with the main tectonic elements and magmatic ages (see text for details). White circles– dated onshore igneous rocks. AP- Abrolhos Magmatic Province. Mu- Mucuri Basin; BB- Besnard Bank; seamounts: Vi- Vitoria; Mo-Monteague; Ja- Jaseur; Da- Davis; Do- Dogaressa; Co- Columbia; Islands: Tr- Trindade and MV- Martins Vaz; RCB- Royal Charlotte Bank; HS-Hot Spur. The fracture zone are from Cande and Labreque (1988). Their prolongation continentwards (grey dashed lines) is hypothetical and based on the projection of the flowline of Rio de Janeiro Fracture Zone (Cande and Labreque, 1988). Offshore structures from Vincentelli et al. (2016); Mohriak (2005) and Ferreira et al. (2014). The onshore structures are from Cavalcante et al. (2019).

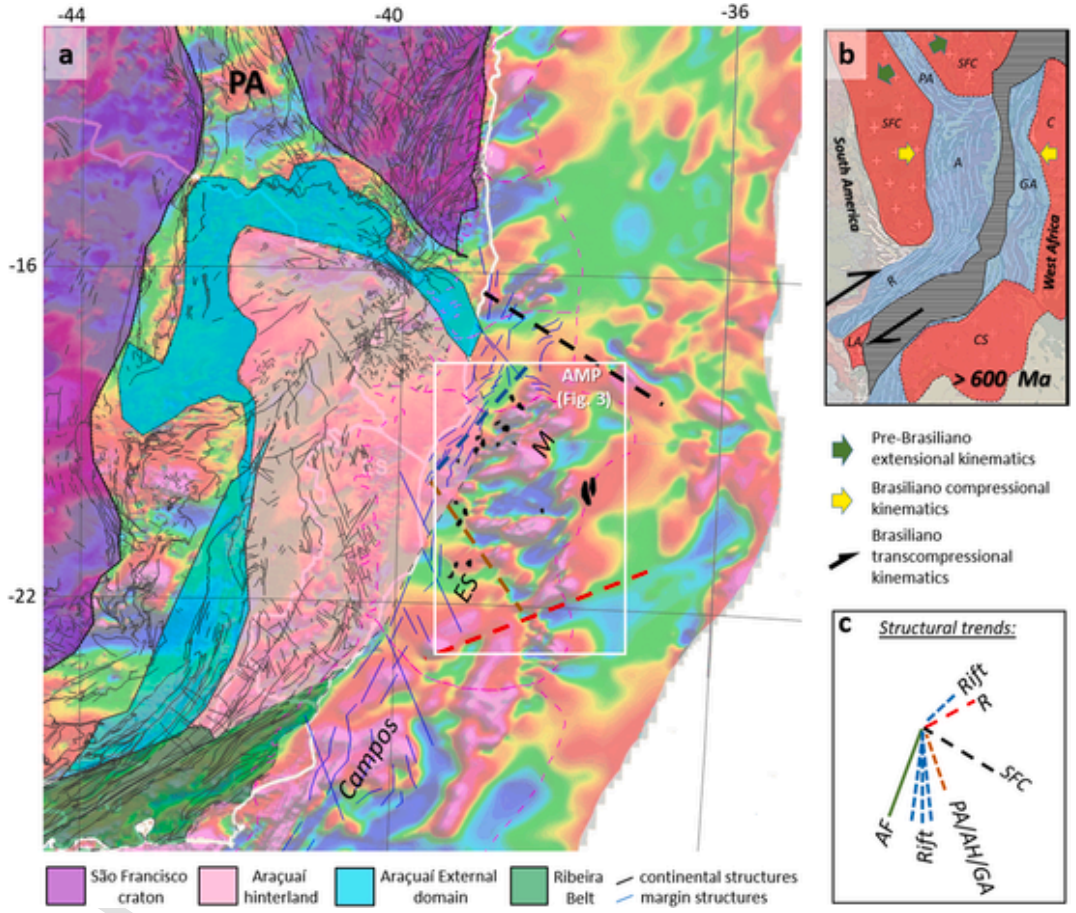


**Fig. 2.** Regional geology of the study area. A) Map of main geological and tectonic features onshore (from CPRM) and rift structures offshore are from Vincentelli et al. (2016); Mohriak (2005) and Ferreira et al. (2014). The magnetic map of the margin is from Correa (2019). The white dashed square shows the location of the Abrolhos Magmatic Province. The onshore structures are from Cavalcante et al. (2019). b) Gondwana reconstruction at ~600 Ma showing the Brazilian and African terranes and kinematics (after Fossen et al., 2017). c) Summary of main structural trends onshore and offshore. M- Mucuri Basin; ES- Espírito Santo Basin; PA- Paramirim aulacogen; R- Ribeira Belt; A- Araçuaí Belt; AH- Araçuaí hinterland; GA- Gabon aulacogen; AF- Araçuaí foreland; SFC- São Francisco Craton; C- Congo Craton; CS- Congo South Craton; LA- Luis Alves Craton.

2009). The opposite occurs for the post-breakup magmatism (Mohriak et al., 2002), with the largest volcanic manifestation represented by the Abrolhos Magmatic Province (AMP) (Chang et al., 1992) at the Espirito Santo and Mucuri basins (Fig. 1, França et al., 2007), followed by the

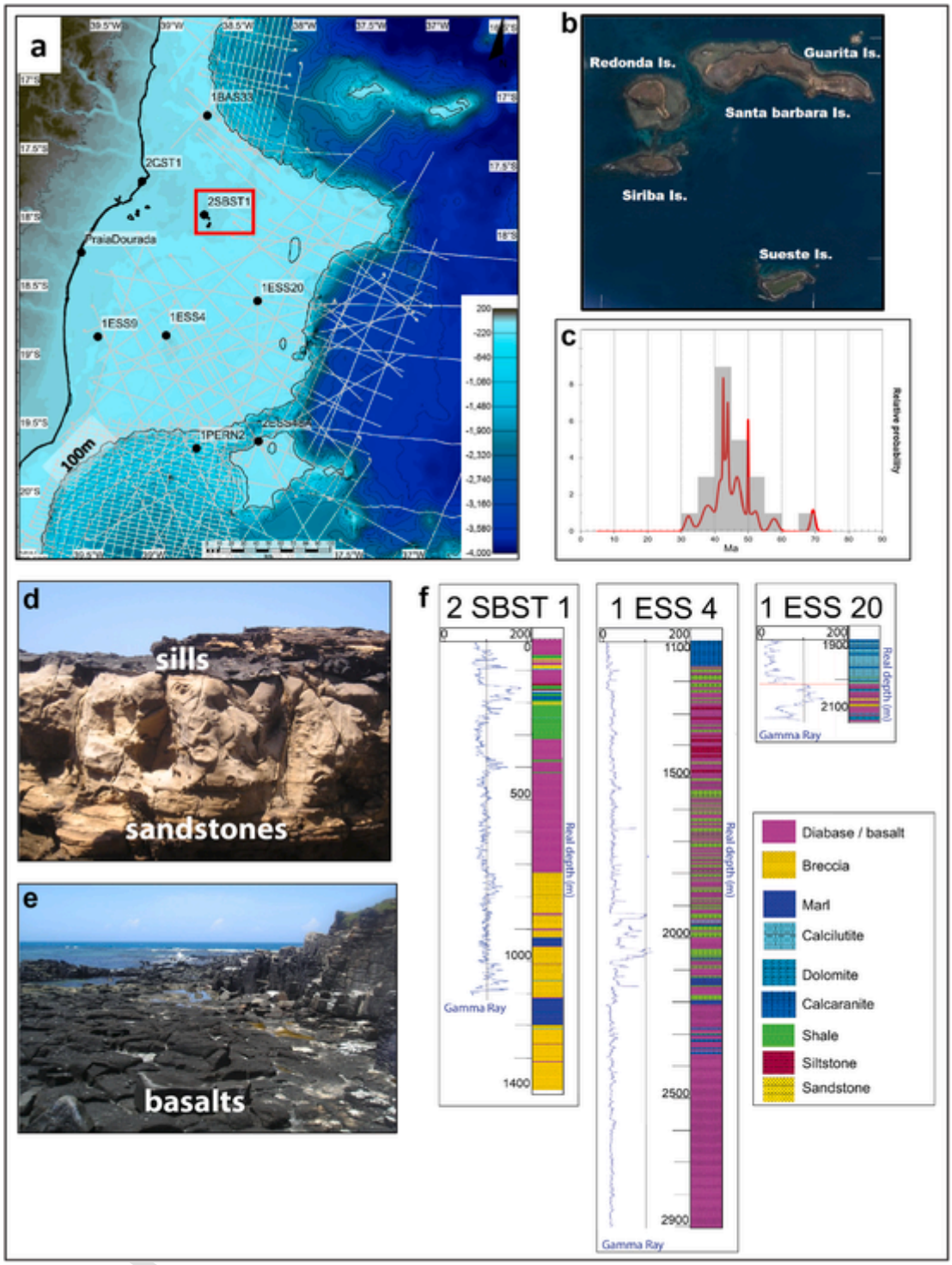


**Fig. 3.** Location of the seismic and well data used in this study. a) Bathymetry map with the location of 2D reflection seismic and well data at the study area. b) Satellite image shows the Abrolhos Archipelago (red rectangle in a). c) Age distribution of published geochronological data (Cordani, 1970; Sobreira and Szatmari, 2003; Mohriak, 2005; França et al., 2007). d) Outcrops showing diabase sills intercalated with sandstones (Santa Barbara Island) and e) showing basalt columnar jointing (Siriba Island). f) The offshore wells used in this study. Depths are in meters below Kelly bushing. (For interpretation of the references to color in this figure legend, the reader is referred to the Web version of this article.)

Cabo Frio High volcanic features (Cainelli and Mohriak, 1999). Thus, the AMP constitutes an example of magmatic reactivation of a passive rifted margin, which started during the Paleogene (Cordani, 1970; Fodor et al., 1989), approximately 40 Ma after break-up of the Espírito Santo Basin (França et al., 2007, Fig. 1).

How the AMP influenced the thermal, tectonic, and stratigraphic evolution of this segment of the Brazilian margin is still poorly understood. There is a debate about the spatial extent of the AMP (Motoki et al., 2014; Sobreira and França, 2006), its duration, and possible origins, with speculations on the existence of a hotspot. This magmatic province was emplaced within different lithospheric domains spanning rifted and thinned continental lithosphere and oceanic lithosphere during a time period of ca. 40 Myr. Additionally, it lies adjacent to an alignment of volcanoes, the Vitória-Trindade Chain (VTC), with magmatic activity

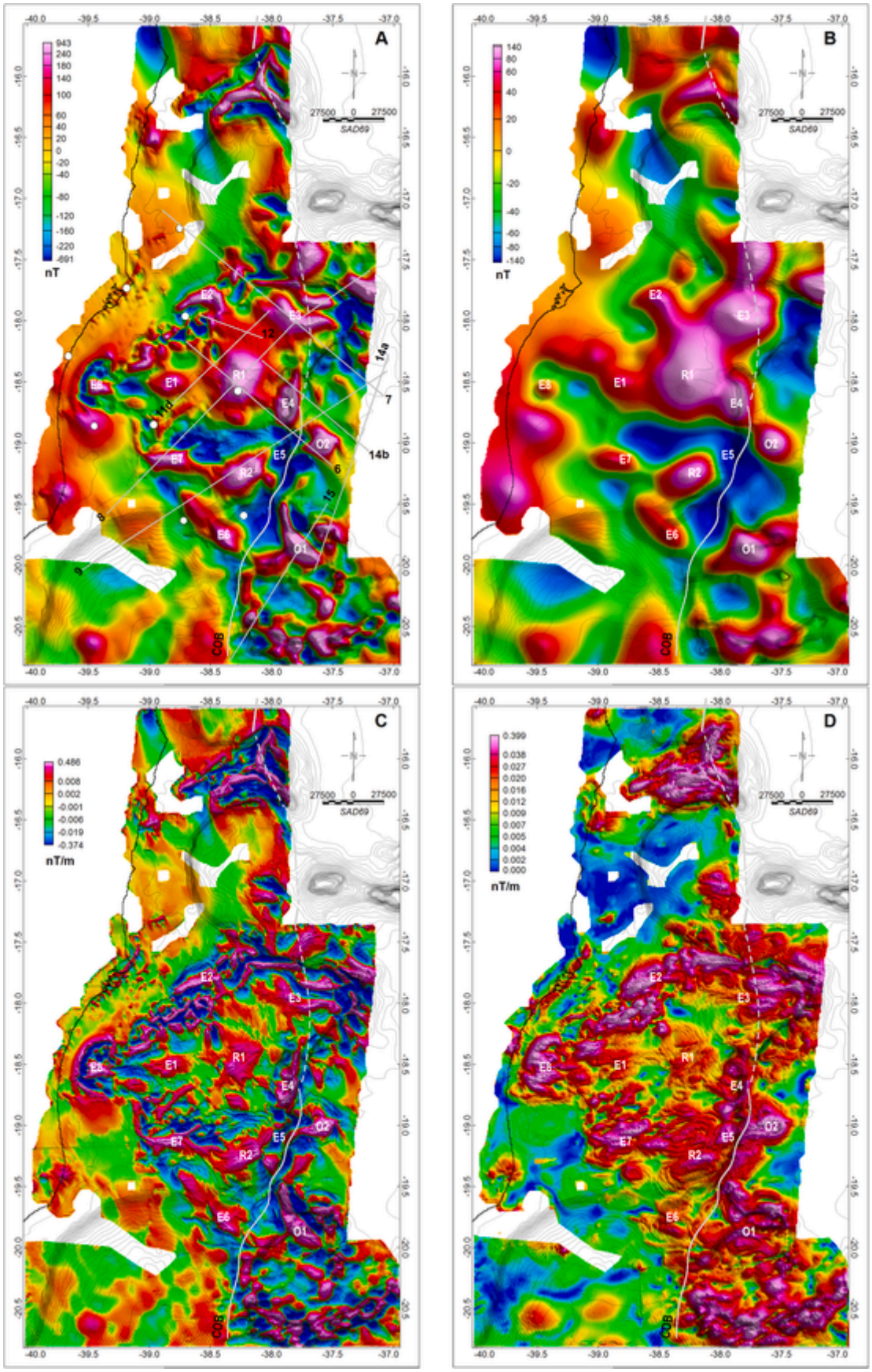
A
B
C
D
nT
nT/m
SAD69
COB
E1
E2
E3
E4
E5
E6
E7
E8
R1
R2
O1
O2
12
14a
14b
7
6
15
8
9

**Fig. 4.** The magnetic anomaly maps. A) magnetic anomaly map Reduced to the Pole (RTP); B) Magnetic anomaly map RTP and upward continued at 10 kms height; C) First vertical derivative of the RTP map; D) Analytical signal of the magnetic anomaly map. Capital letters with numbers-identify main anomalies identified in this study; grey lines-location of the seismic sections and their respective figures; circles-wells used in this study that recovered basalts. The continuous white line represents the observed COB and the white dashed line is the estimated COB mapped in this work; dark grey contours-bathymetry.

**Table 1**
Physical properties of each layer in the 2D forward models.

| Lithologies | Physical properties | | |
|---|---|---|---|
| | D (kg/m$^3$) | K (SI) | NRM |
| Water | 1030 | 0 | – |
| Sediments | 2300–2500 | 0 | – |
| Upper crust | 2670 | 0.0001 | – |
| Lower crust | 2870–2900 | 0 | – |
| Mantle | 3300 | 0 | 0 |
| Basalts (Normal magnetization) | 2750–2800 | 0.01–0.03 | 1–2 |
| Basalts (Reverse magnetization) | 2750–2800 | 0.01–0.03 | 1–2 |
| Magmatic underplating | 2900–3000 | 0.02 | – |
| Oceanic crust | 2850 | 0.01–0.02 | – |

from Oligocene to Pleistocene (Pires et al., 2016). Some key questions that guide this work are: what is the extension and the structure of the AMP? What was the mechanism of its formation and what is its relationship with the VTC?

This contribution presents a detailed analysis of the AMP, based on extensive geophysical mapping using reflexion seismic integrated with new high-resolution magnetic maps and boreholes. The aim of this work is to investigate its morphostructure, spatial distribution and timing, and discuss its significance for the margin evolution and origins. We show the existence of igneous edifices of various sizes, emplaced at different depths and discuss how their emplacement modified the pre-existing Cretaceous rifted margin. Our findings suggest that the magmatism that created the AMP was a long and widespread process, possibly associated with a differentiated thermal structure and may contribute to the understanding of other global volcanic complexes.

### 1.1. Regional setting

The offshore Espírito Santo and Mucuri basins located at the eastern Brazilian margin (Fig. 1) formed during the Gondwana break-up in Lower Cretaceous. The stratigraphic record of these basins can be divided into four main units: crustal basement, rift, post-rift, and drift super-sequences (França et al., 2007).

- The Crustal Basement

The crystalline basement comprises Proterozoic/Cambrian metamorphic and granitoids rocks from the Araçuaí orogen (Fig. 2). The Araçuaí and conjugate West-Congo orogens in Africa originated during the assembly of West Gondwana (Brazilian orogeny). The Araçuaí is part of the Mantiqueira Province (Almeida et al., 1973; Bento dos Santos et al., 2015 and references therein) and registered a complex evolutionary process involving pre, syn and post collisional deformational events (Alkmim et al., 2006; Cavalcante et al., 2019) with the western margin of the São Francisco Craton in the Neoproterozoic. This Orogen comprises three different crustal domains (Fig. 2): 1) the pre-collisional Paramirim aulacogen constituted by reworked basement (Cruz and Alkmim, 2017). It is a long-lived pre-Brasiliano extensional basin, NW-SE oriented that transects the São Francisco Craton. It was inverted during the Brasiliano orogeny and show evidence of extensional and transcurrent post orogenic kinematics (Cruz et al., 2015); 2) the external domain (or foreland) comprising fold-and-thrust belt of supracrustal, arc complexes and reworked basement; 3) a wide and hot internal domain (or hinterland) characterized by anatexis and magmatism (Tack et al., 2001; Heilbron et al., 2008; Pedrosa-Soares et al., 2008; Fossen et al., 2017). The Araçuaí orogen displays N–S to NW-SE structural trends and a progressive increase from low-grade metamorphism in the foreland to a high temperature–low-pressure metamorphism in the hinterland (Fossen et al., 2017).

The Ribeira orogen to the south is characterized by a major strike-slip system of anastomosing transcurrent shear zones-oriented NE-SW (Heilbron et al., 2000; Fossen et al., 2017 and references therein). The shear zones separate domains of thrusted and folded rocks controlled by a transpressional combining orogen-parallel strike slip and orogen-normal thrusting kinematics. The transition from the Araçuaí to Ribeira (to the south) orogenic belts is characterized by a series of transcurrent shear zones (Alkmim et al., 2017; Hasui and Oliveira, 1984; Heilbron et al., 2000; Pedrosa-Soares et al., 2001; Trompette, 1994; Vauchez et al., 2007).

- **The Espírito Santo and Mucuri basins**

The formation of the northern Espírito Santo and Mucuri basins in Early Cretaceous involved the extension of the complex Araçuaí orogen (Fig. 2). It was controlled by the São Francisco craton to the north, by the external and hinterland domains of the Araçuaí orogen to the west and the Gabon aulacogen to the east. During the Lower Cretaceous the rifting developed orthogonal grabens/half grabens oriented N–S and NNE-SSW (Fig. 2).

The first igneous rocks of the basin are represented by the Cabiúnas Fm., constituted by tholeiitic basalts, with radiometric ages between 118 and 136 Ma (França et al., 2007, Fig. 3), which intruded syn-rift deposits. The rift sequence (Valanginian to Lower Aptian) is constituted by fine-grained lacustrine rocks, fluvio/fan delta deposits along the rift faults and carbonates at the inner structural highs. The transitional, late syn-rift (distal) to early post-rift (proximal) Middle Aptian a siliciclastic rocks and thick Late Aptian evaporates deposited in fluvio-deltaic and sabkha environments (França et al., 2007). The salt deposits comprise Anhydrite and Halite and are mainly developed at central and southern Espírito Santo Basin, with thickness varying from less than 50 m in shallow waters to large salt diapirs and walls of up to 5000 m in deep waters (França et al., 2007). The halokinesis affect the post-salt sequences, controlling the deep-water deposits and being responsible for the formation of the hydrocarbon fields.

After the breakup, the marine phase comprises three super-sequences: (1) Albian siliciclastic shelf and carbonates deposited in a neritic environment of a shallow and restricted narrow sea; (2) a Cenomanian to Lower Eocene transgressive marine system characterized by siliciclastic and marls; and (3) an Upper Eocene to recent regressive system that comprises coarse-grained sandstones, platform carbonates, distal mudstone and deep water deposits (Chang et al., 1992), reaching a maximum thickness of 5000 m (França et al., 2007).

The northern Espirito Santo and Mucuri basins were widely affected by the emplacement of the AMP. It overprinted the basins physiography and influenced the Paleogene and younger depositional sequences. At Lower Eocene, the volcanism associated with the Abrolhos Fm. resulted in regional uplift, increased siliciclastic input and formation of a shallow carbonate platform on the top of the volcanic highs (França et al., 2007). The Eocene sequences are highly intruded by the igneous rocks of the AMP, which outcrop at the Santa Barbara, Siriba, Guarita, Redonda and Sueste islands and at onshore (França et al., 2007) (see location on Fig. 3).

- Geodynamic Context

**Table 2**
Summary of magnetic and seismic characteristics of the individual anomalies identified in this study.

| Anomaly | Magnetic analysis and modeling | | | Seismic interpretation | | Margin Domain | Figure |
|---|---|---|---|---|---|---|---|
| | Type | Shape | Depth (km) | Geomorphology & area | Tectonostratigraphic relationship | | |
| **R1** | Normal polarity; long-wavelength (~60 km) and high amplitude anomaly (~490 nT) | Wide and semi-circular; connects laterally to E1, E2, E3 and E4 | Deep seated sources (~3–8) | Knobbed mushroom-like cross-section (~1782 km$^2$) | Post-Eocene compaction anticlines on top; stem-like root with irregular walls and sediment-igneous interfingering | Distal margin | 6, 8, 10 |
| **R2** | Normal and reverse polarity; short- and middle-wavelength (5–50 km) and high amplitude anomaly (~400 nT) | semi-circular anomaly, surrounded by "Terrace" and small circular anomalies; connects laterally to E5, E6 and E7 | Shallow and deep-seated sources (~2–7) | Tabular-like cross sectional shape with two lateral arms (~2859 km$^2$) | Intrusion forced folding of Eocene surface on top. Onlap of Oligocene sequence. Lateral connections to E5 and E6 anomalies | Distal margin | 9 |
| **E1** | Normal polarity; middle and short wavelength (5–35 km) and middle amplitude anomaly (~250 nT) | Wide and semi-circular to elongate shape | Shallow and deep-seated sources | Dome-like cross sectional shape (~941 km$^2$) | Intrusion forced folding of Eocene surface on top & normal drag of host rock | Necking zone | – |
| **E2** | Normal and reverse polarity; middle and short-wavelength (~10–30 km) and high amplitude anomalies (~460 nT) | Elongate shape, semi-linear and composite anomaly | Shallow and deep-seated sources (~0–5) | Biconvex lense-like cross sectional shape (~1070 km$^2$) | Intrusion forced folding of Eocene surface on top & normal drag of host rock | Necking zone | 12 |
| **E3** | Normal and reverse polarity; middle and short-wavelength (~10–50 km) and high amplitude anomalies (~360 nT) | Elongate anomaly | Shallow and deep-seated sources (~1–4) | Biconvex lense-like cross sectional shape (~1581 km$^2$) | Intrusion forced folding of Eocene surface on top & normal drag of host rock Vents at top of body | COB | 7,8 |
| **E4** | Normal and reverse polarity; middle and short-wavelength (~10–30 km) and high amplitude anomalies (~460 nT) | Elongate anomaly, surrounded by "terrace" anomalies | Shallow and deep-seated sources (~2–6) | Dome-like cross sectional shape (~1352 km$^2$) | Vents at body's flank; normal drag of host rock | COB | 6, 14b |
| **E5** | Reverse polarity; middle-wavelength (20 km) and high amplitude anomaly (~-460 nT) | Semi-Linear anomaly. It connects with the adjacent R2 and O2 | Shallow seated sources (~2) | Biconvex lense-like cross sectional shape (~334 km$^2$) | Normal drag of host rock; vents at the top. Connected to R2 anomaly | COB | 9 |
| **E6** | Normal polarity; middle-wavelength (30 km) and high amplitude anomaly (150–300 nT) | Linear anomaly, surrounded by the "Terrace" anomalies | Deep seated sources (~5) | Biconvex lense-like cross sectional shape (~1835 km$^2$) | Intrusion forced folding of Eocene surface on top. Connected to R2 anomaly | Distal margin | 9 |
| **E7** | Normal and reverse polarity; short and middle-wavelength (~5–30 km) and high amplitude anomalies (~-300-400 nT) | Linear anomaly; connects laterally with small circular anomalies; is surrounded by "Terrace" anomalies | Shallow and deep-seated sources (~2.5–5) | Biconvex lense-like cross sectional shape (~1875 km$^2$) | Intrusion forced folding of Eocene surface on top. Onlap of Oligocene and Lower Miocene sequences. Normal drag of host rock at flanks | Necking zone | 8 |
| **E8** | Normal and reverse polarity; short-wavelength (~5–15 km) and high amplitude anomalies (~-470-400 nT) | A semi-circular anomaly, surrounded by a "half-circle" and several small anomalies | Shallow and deep-seated sources | Complex shape, including isolate cones, stacked-cones, and plano-convex bodies (~1742 km$^2$) | Intrusion forced folding of Eocene surface on top; drag of host rock. Igneous intrusions at the clinoforms of the Cretaceous shelf edge | Proximal margin | – |
| **O1** | Normal and reverse polarity; short- and middle-wavelength (~5–20 km) and high amplitude anomalies (~700 nT) | Linear anomaly, surrounded by the "Terrace" and small circular anomalies | Deep and shallow seated sources | Flat-top conical shape (guyot) (~3375 km$^2$) | Thick (~3 km, well 2ESS48A) carbonate platform on top. Step-like walls (producing terrace anomalies), Cross cut the oceanic sediments | Oceanic Domain | 14a, 15 |
| **O2** | Normal and reverse polarity; middle-wavelength (~30 km) and very high amplitude anomalies (~770 nT) | Circular shape; is surrounded by the "Terrace" anomalies | Deep seated sources (~4–7) | Conical shape (~1437 km$^2$) | Drag of host rock at body flanks | Oceanic Domain | 6, 9 |



The AMP represents the largest post-break magmatic structure of the Brazilian margin (Chang et al., 1992), emplaced onto both continental and oceanic lithospheres. It lies adjacent to the VTC, a linear volcanic chain on oceanic crust that extends for 1100 km eastward from the Besnard Bank at the southeastern border of the AMP (Fig. 1). The VTC comprises thirty seamounts reaching 4–5 km above regional bathymetry and five volcanic islands with rugged topography (Almeida, 2006; Motoki et al., 2012; Santos et al., 2018). The VTC displays a progression of radiometric and paleontological ages from west to east, ranging from 34 Ma to 0.3 Ma (Fig. 1; Siebel et al., 2000; Pires et al., 2016; Santos et al., 2018 and references therein). Petrographically, the VTC is mainly constituted by volcanic rocks with ultramafic to intermediate composition and alkaline affinity (Santos et al., 2018). The formation of the VTC immediately followed the AMP magmatism, advocating a possible relationship between these igneous features.

A hypothesis for the origin of the AMP and the VTC provinces proposed by previous works is related to the passage of the South American plate over a mantle plume during the Upper Cretaceous to Tertiary, assuming a stationary hotspot presently located under or near the Trindade-Martin Vaz Islands (Herz, 1977; Morgan, 1983; Hartnady and Le Roex, 1985; O'Connor and Duncan, 1990). Later, Morgan (1983) and O'Connor and Duncan (1990) extended the activity of the mantle plume to Upper Cretaceous, correlating it with the formation of the onshore alkaline provinces of Poxóreu, Iporá and Alto Parnaiba (Fig. 1). Gibson et al. (1995) proposed that these alkaline provinces formed by the impingement of a mantle plume in the Late Cretaceous (~85 Ma) under

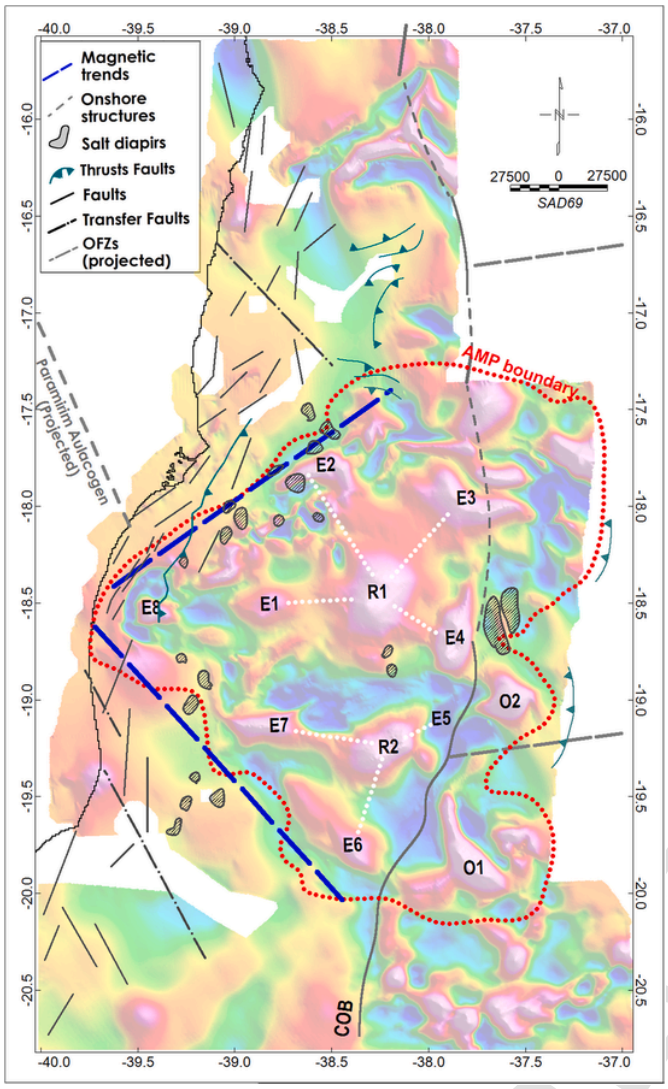


**Fig. 5.** a) Interpreted magnetic anomaly map RTP, showing the correlations between the magnetic trends and pre-existing onshore and offshore structures at the AMP.

the southeast Brazilian continental lithosphere, along the continental Proterozoic Brasília Belt, which would have acted as a "thinspot" for the mantle upwelling. According to these authors, the re-emergence of the magmatism offshore would have formed the Abrolhos Magmatic Province, and later the VTC, by the westward drift of the South American plate. Alternatively, Thompson et al. (1998) and Siebel et al. (2000) proposed a deflection of the so-called Trindade plume southwards from Upper Cretaceous to Eocene (~80–50 Ma) due to the passage of the São Francisco Craton over the plume, suggesting a link between the magmatism of the VTC, the AMP and the alkaline rocks of the Serra do Mar Province (Fig. 1). That hypothesis is mainly based on the eastward age progression and the geochemical signature of trace elements and isotopes that correlates the VTC and ocean island basalts as generated by partial melting of a fertile mantle source (Santos et al., 2018).

Other alternative explanations for the AMP interpret this major tectonic feature as associated with an oceanic fracture zone that links the VTC with the South Atlantic spreading center (Ferrari and Riccomini, 1999; Mohriak, 2003; Alves et al., 2006). Assumpção et al. (2004) proposed that weakness zones in the crust generated fracture zones, which associated with thermal anomalies would have served as magmatic conduits.). Fig. 1 displays the continentward prologation of the oceanic fracture zones across the AMP and VTC area, named the $16^0$, the Santa Helena and the Trindade (previously named Hotspur) fracture zones, based on Cande and Labreque (1988) flowlines. It is possible to notice that the orientation of the southern portion of the Abrolhos Platform and of some segments of the VTC show a close relationship with the fracture zones trends. However, there is an orientation mismatch between the AMP (semi-circular shape), the linear VTC (~E-W) and the absolute motion of the South American Plate (~NW) as indicated by the plate reconstruction of Heine et al. (2013).

### 1.2. The igneous rocks of the Abrolhos Magmatic Province

The Igneous rocks of the AMP have been recovered from outcrops and wells onshore, and offshore along the Abrolhos Platform, as well as from outcrops at the Abrolhos Archipelago (Fig. 3a).

Compositionally, the AMP is bimodal. The basic igneous facies are more abundant and comprise basalts, trachybasalt, basanites, tefrites, diabase, ultrabasic cumulates and basic volcaniclastic rocks (Fodor et al., 1989; Arena, 2008). Basic facies have been reported in onshore and offshore wells and in the Abrolhos Archipelago outcrops. The basic facies found in the Abrolhos Archipelago are interbedded with sedimentary rocks, except for Sueste Island where only magmatic rocks are observed above sea-level (Cordani, 1970; Arena, 2008). The basic facies in the archipelago are composed of Olivine-Plagioclase basalt, Pyroxene-Plagioclase-Olivine basalt, Pyroxene-Plagioclase basalt, and Cumulates (Arena, 2008), displaying diabase sills (Fig. 3b and c, Santa Barbara Island) and prismatic columnar disjunction of basaltic lavas (Fig. 3b and e, Siriba Island; Mohriak, 2005; Arena, 2008). Field work at the Abrolhos Archipelago by Arena (2008) indicate a gently folded N–S bearing magmatic and sedimentary units. Additionally, Arena (2008) identified NNE-SSW and NNW-SSE compressive and transpressive faults, as well as ENE-WSW normal faults and joints indicating local E-W and ENE-WSW compressive stress systems.

The onshore well 2CST1 and the offshore wells 2SBST1, 1ESS4, 1ESS20, 1PRN2, 2EES48A (Fig. 3a and f) sampled the AMP igneous rocks. Both onshore and offshore wells penetrated volcanic and volcaniclastic rocks with intercalations of clastic sediments and carbonates (Mohriak, 2005; Sobreira and França, 2006; Novais et al., 2008; Gomes and Suita, 2010; Oliveira et al., 2012, 2018). The well 2SBST-1 drilled approximately 1400 m of volcanic and volcaniclastic rocks in Santa Barbara Island (Fig. 3f). It sampled 675 m of volcaniclastic rocks intercalated with carbonates, overlained by 725 m of diabase dykes and sills intercalated with siliciclastic rocks (Mohriak, 2005). The descriptions of this well included: reddish levels of hematite interpreted as subaerial exposure of the volcanic rocks (Mizusaki et al., 1994); pyroxene-phyric diabases at 620–709 m depth (Fodor et al., 1989); ultramafic cumulates at 573 m depth (Cordani, 1970; Fodor et al., 1989). The well 1ESS20 displays an upper 1930-m-thick unit of carbonate deposits formed during the Lower Eocene to Lower Miocene, based on foraminifera interpretations (ANP) and overlies 126 m thickness of volcanic rocks. The volcanic sequence starts with a vesicular grey-reddish basalt, with variable degrees of weathering and intercalated with dolomites and sandstones and passes to acid rocks on top of the sequence. (Fig. 3d; Gomes and Suita, 2010).

The well 1ESS4 recovered 1100 m of carbonates with siliciclastic intercalations (ANP) followed by 1210 m of weathered fine-grained, brown-reddish vesicular basalts and volcanic glass fragments, densely intercalated with marls, shale and calcilutite (Fig. 3f), with 540 m of massive black basalt at its base. The intercalation of basalt and volcanic glass fragments with sedimentary rocks may be indicative of sub-aerial exposure of the upper part of this magmatic unit, related to volcaniclastic processes. Basic facies have been reported in wells CST1 (basalt intercalated with sediments; Cordani and Blazekovic, 1970), 1ESS9 (diabase, Fodor et al., 1989) and 1BAS33 (wehrlite, Fodor et al., 1989). The presence of pyroclastic rocks was observed onshore at Caravelas region and at offshore wells 2-SBST-1 and 1-PRN-2, interpreted as subaquous

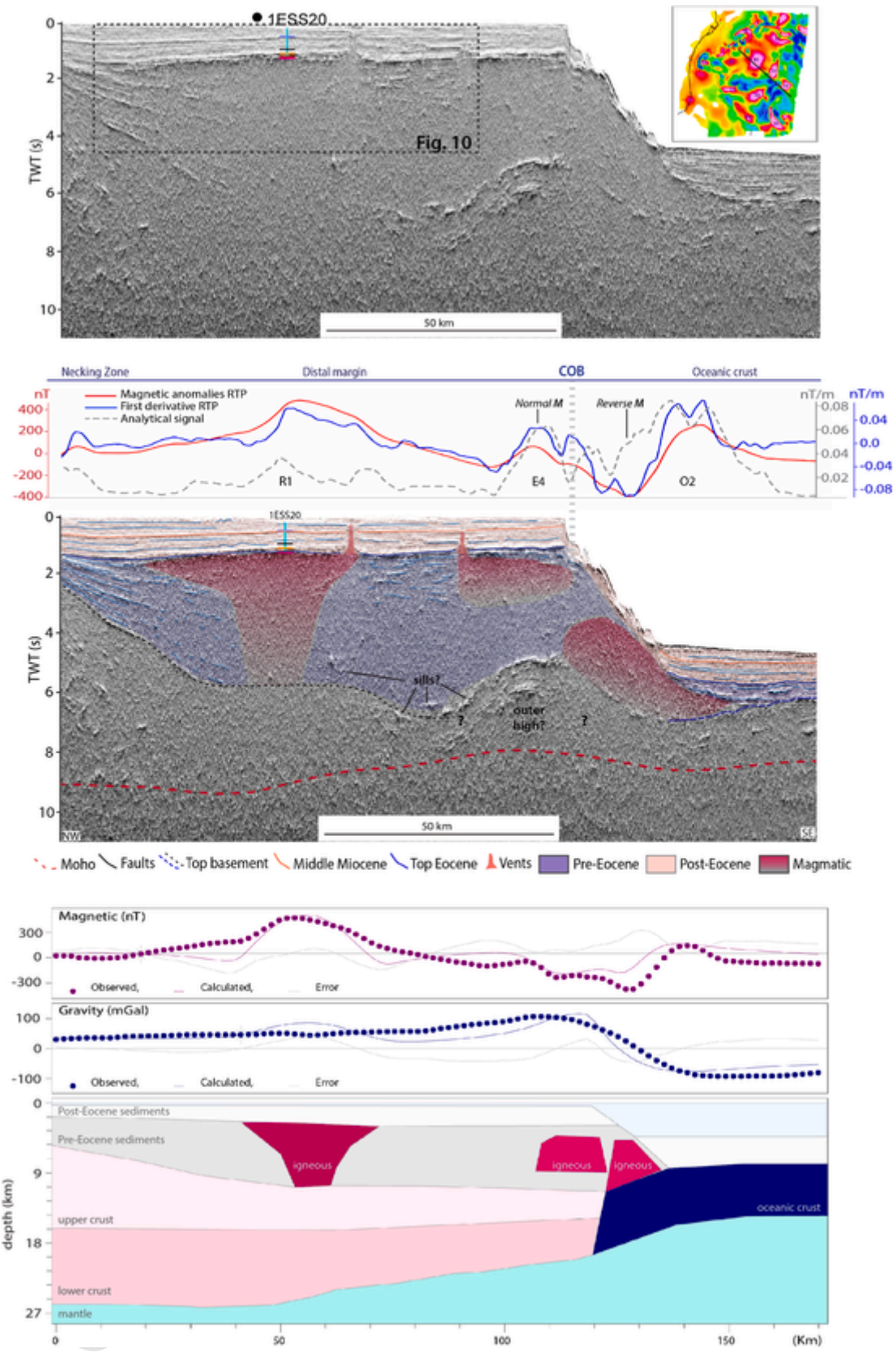


**Fig. 6.** The seismic section uninterpreted and interpreted (top) and the correspondent 2D forward model (bottom). For block parameters, see Table 1 and location in Fig. 4A. Coloured lines on the well represent the stratigraphic levels: magenta- Top of Abrolhos Fm., orange- Eocene Unconformity, black- Oligocene, purple- Miocene. (For interpretation of the references to color in this figure legend, the reader is referred to the Web version of this article.)

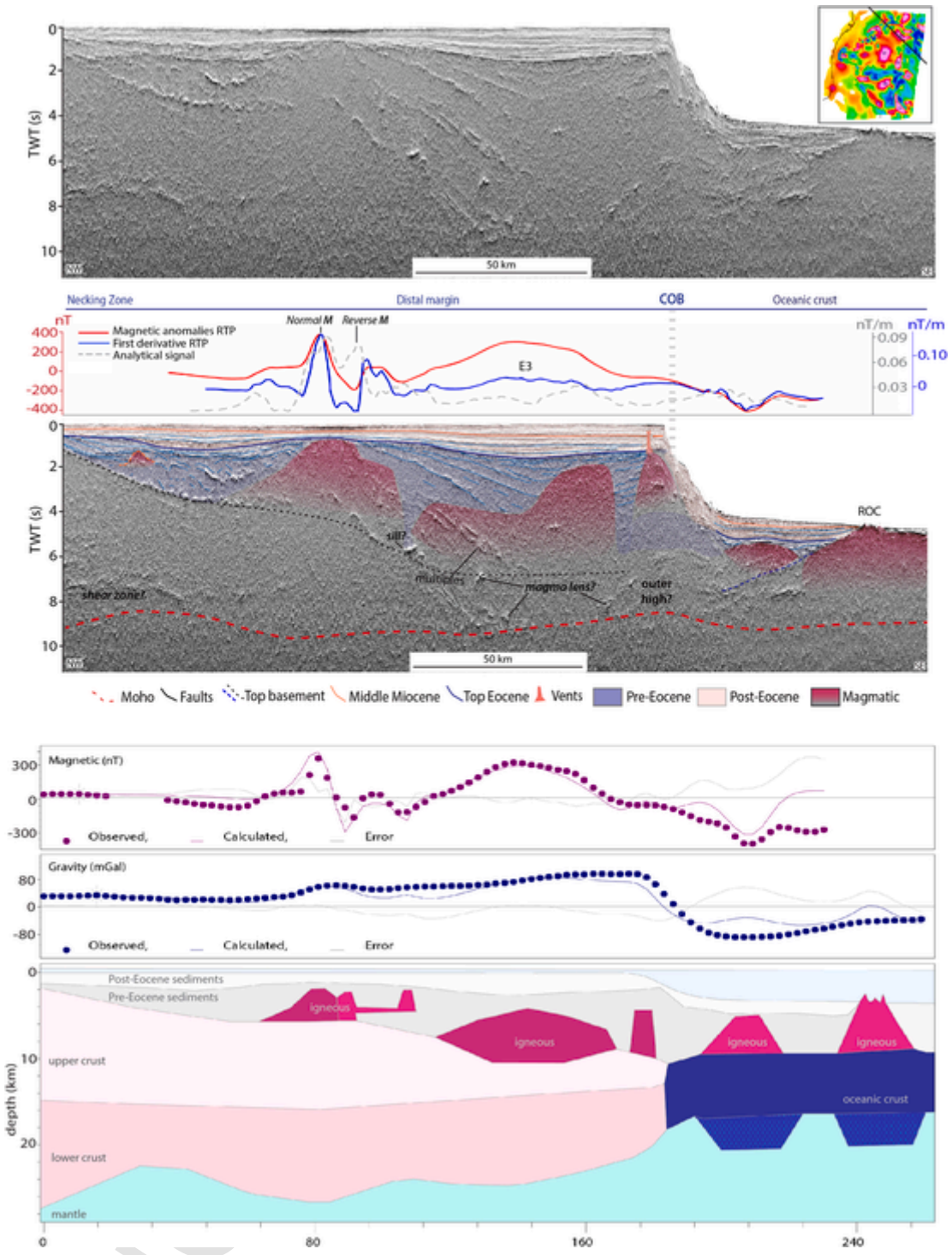


**Fig. 7.** The seismic section uninterpreted and interpreted (top) and the correspondent 2D forward model (bottom). For block parameters, see Table 1 and location in Fig. 4A. Coloured lines on the well represent the stratigraphic levels: magenta- Top of Abrolhos Fm., orange- Eocene Unconformity, black- Oligocene, purple- Miocene. (For interpretation of the references to color in this figure legend, the reader is referred to the Web version of this article.)

volcanism at the beginning of the Abrolhos magmatism (Oliveira et al., 2018).

The subordinate acid facies of rhyolite, trachyte and volcaniclastic rocks are reported at onshore outcrops and offshore wells. Rhyolitic and ignimbrite rocks occur over the São Mateus crystalline basement onshore (Fig. 1), dated as 69 Ma (Fodor et al., 1989; Sobreira and França, 2006; Novais et al., 2008; Gomes and Suita, 2010; Oliveira et al., 2012, 2018). The Praia Dourada outcrop (Oliveira et al., 2012, Fig. 3a) is characterized by sub-aqueous pyroclastic eruptions of rhyolitic composition interbedded with sediments of the Rio Doce Formation. Offshore wells 1ESS20 and 1BAS 117 drilled trachytes and rhyolites overlying basalts. The presence of trachyte xenoliths in the rhyolitic facies was interpreted as indicative of normal crystallization order and fractional crystallization differentiation (Sobreira and França, 2005).

Geochemically, the AMP rocks display a transitional to alkaline affinity with high $TiO_2$ (Fodor et al., 1989; Sobreira and França, 2006; Arena, 2008). Isotopic and trace-element composition indicate that the

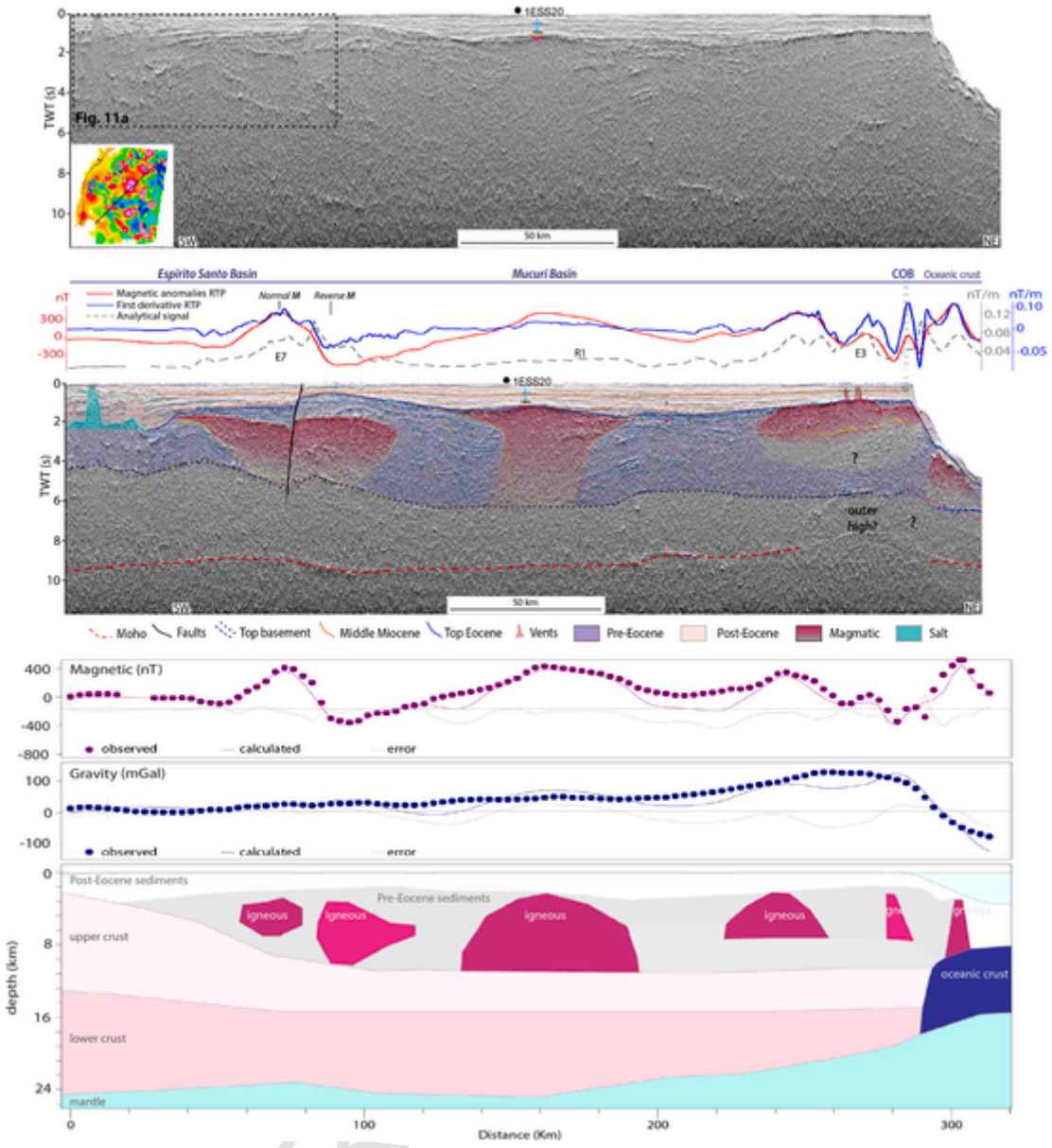


**Fig. 8.** The seismic section uninterpreted and interpreted (top) and the correspondent 2D forward model (bottom). For block parameters, see Table 1 and location in Fig. 4A. Coloured lines on the well represent the stratigraphic levels: magenta- Top of Abrolhos Fm., orange- Eocene Unconformity, black- Oligocene, purple- Miocene. (For interpretation of the references to color in this figure legend, the reader is referred to the Web version of this article.)

AMP formed via partial melting of a fertile mantle source (Fodor et al., 1989; Arena, 2008).

The geochronological data (K/Ar and Ar/Ar) of the AMP (Fig. 3c) shows a range from 32 to 69 Ma (Cordani, 1970; Sobreira and Szatmari, 2003; Mohriak, 2005; França et al., 2007). The large age dispersion reflects the temporal evolution of this province and analytical difficulties (differences in radiometric techniques and geochronological laboratories).

## 2. Material and methods

We use aeromagnetic, 2D reflection seismic data and exploration wells to study the nature and spatial distribution of the AMP. The magnetization of the source layers was constrained as much as possible by the works of Montes-Lauar (1993), Ernesto et al. (2005) and Ernesto (Personal communication, 2020). We use reflexion seismic data to help to locate the depth, edges and constrain the morphology of the magnetic sources.

### 2.1. Seismic data and wells

The Espírito Santo and Mucuri basins seismic reflection data set comprises long offset 2D seismic lines (Fig. 3a) with 8–12 s of recording length, 4 msec sampling rate processes in pre-stack time and post-stack time migration. We used six exploratory wells for lithological description, regional correlation and time/depth calibration (Fig. 3a), courtesy of the Brazilian National Agency of Petroleum, Gas and Biofuels (ANP). To investigate the AMP we selected key regional seismic sections (Fig. 4a) and applied a blend of standard amplitude sections with RMS (Root Mean Square) and tecVA attributes (Bulhões and De Amorim, 2005), in order to enhance the seismic facies identification. The application of seismic attributes highlights large amplitude contrast and is a useful tool to interpret the distribution of igneous rock hosted in the siliciclastic sequences. The differences in the reflectivity patterns has been used as a criteria for the separation between siliciclastic (parallel to subparallel seismofacies) and igneous rocks (reflection-free seismofacies) due to the fact that there is not a specific reflector associated with this inter-

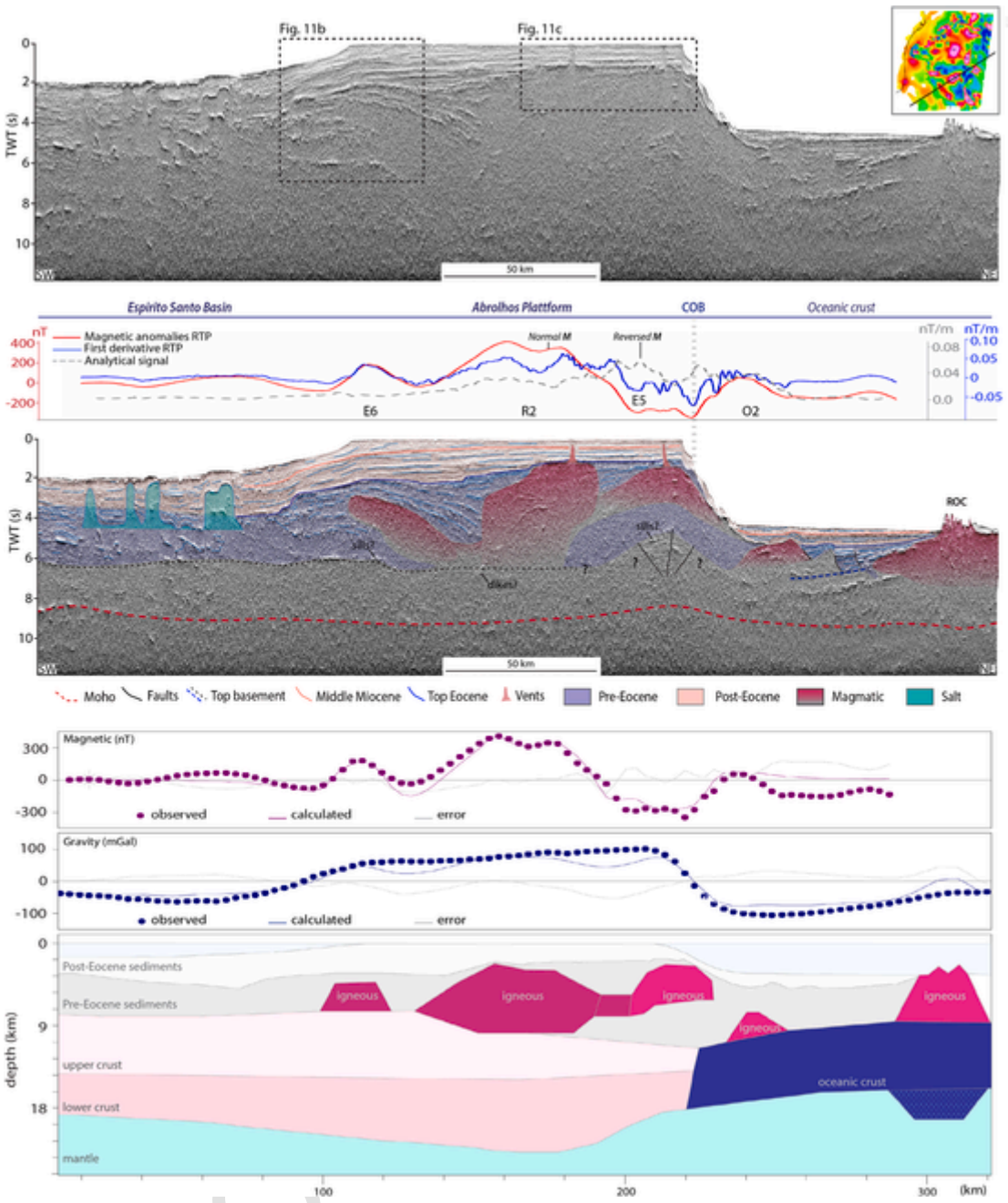


**Fig. 9.** The seismic section uninterpreted and interpreted (top) and the correspondent 2D forward model (bottom). For block parameters, see Table 1 and location in Fig. 4A. Coloured lines on the well represent the stratigraphic levels: magenta- Top of Abrolhos Fm., orange- Eocene Unconformity, black- Oligocene, purple- Miocene. (For interpretation of the references to color in this figure legend, the reader is referred to the Web version of this article.)

face. A horizon separating both seismofacies (named as Top Abrolhos) was mapped, and two reflectors corresponding to the Top Eocene Unconformity, and Mid Miocene unconformity have been mapped in the area of study. There are no individual continuous reflectors that represent those unconformities, which were characterized in this study by differences in reflection patterns and by truncating horizons below and onlap relationship above. The check shot data and synthetic seismograms from wells 1ESS4 and 1ESS20 for well/seismic tie used in this study are from Cardozo (2018).

The presence of large igneous edifices resulted in an important deterioration of the seismic signal for the pre-Eocene sequences and thus the interpretation of deeper horizons such as Top Basement and Moho was partially speculative.

### 2.2. Aeromagnetic data

The magnetic data is sourced from four aerosurveys from the ANP public database. The data processing was carried out using Oasis Montaj V9.0. The individual survey acquisition parameters are: survey 0401_MAG_app_050_ES_JEQUITINHONHA (1979, 700 m flight height and 4000 m line spacing), survey EMAG01_BM_ES_1_2 and survey EMAG01_BM_ES_3 (1999, 300 m flight height, N30W direction and 4000 m line spacing), and survey app_270 (1990, 500 flight height, N30W direction and 3000 m line spacing). Due to their acquisition differences, each survey was treated separately for removal of the Regional Magnetic Field (IGRF models). The surveys were leveled, reprojected to the same coordinate system, interpolated at 250 × 250 m interval and upward continued at 500 m altitude. All grids were knitted

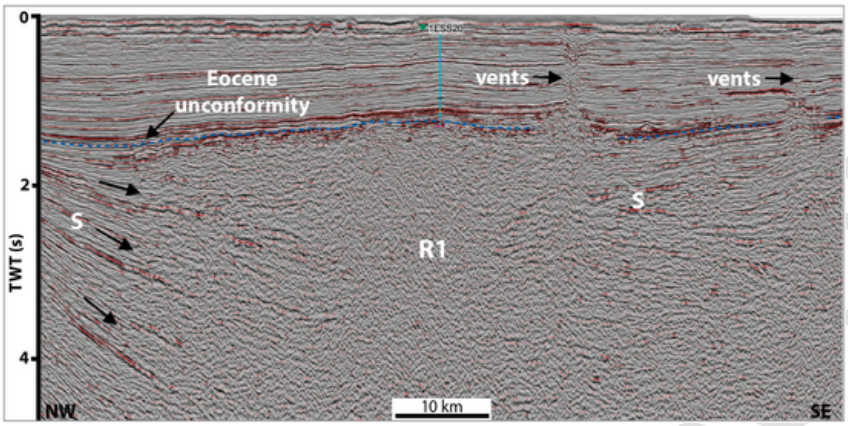


**Fig. 10.** Detail of seismic section. Anomaly R1 was drilled by well 1ESS20 that recovered basalts and display a reflection-free seismofacies, that passes laterally into more reflective seismofacies with parallel/subparallel and divergent reflection interpreted as sedimentary rocks. Vents on SE side affect up to Middle Miocene strata. See location on Fig. 4A.

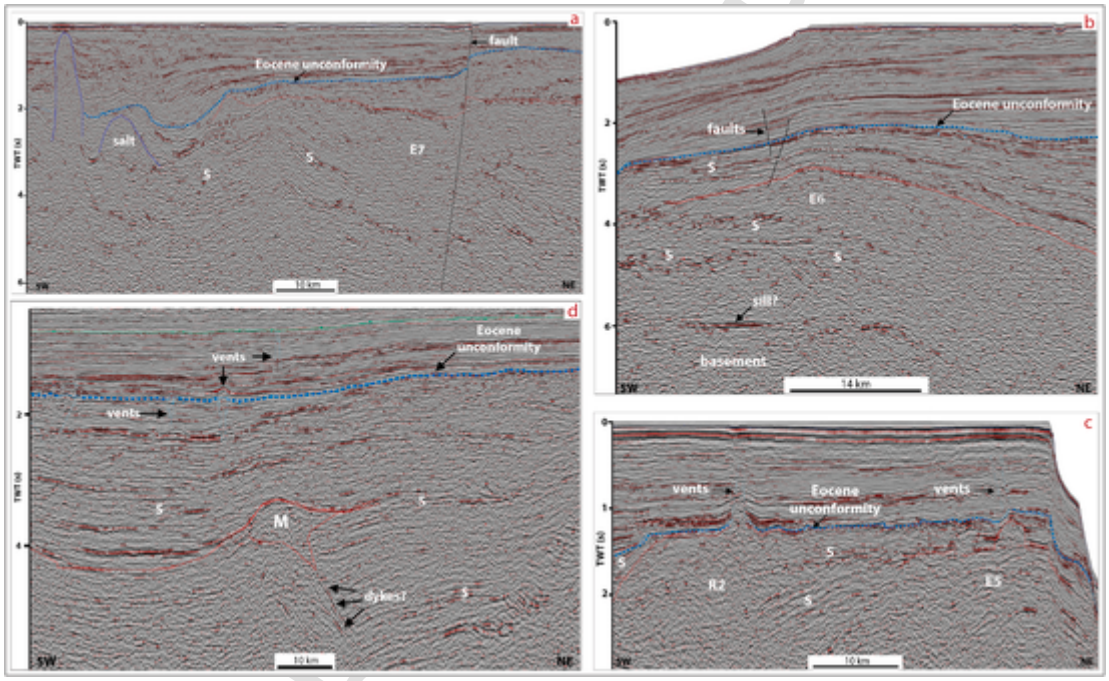


**Fig. 11.** Detail of seismic sections. a) Igneous edifice associated with magnetic anomaly E7 overlying sedimentary rocks (S) and cut by a subvertical fault. b) igneous edifice associated with magnetic anomaly E6 overlying sedimentary rocks (S) intruded by sills. c) Seismofacies variation between the igneous edifices R2 and E5 and with the surrounding sedimentary sequences (S). Note vents affecting younger sequences. d) Magmatic body (M) over a feeding structure – dykes intruding sedimentary rocks (S). For locations see Fig. 4A.

together using the suture method and then trended to each other, i.e., the trends are calculated based on all the grids being stitched together. The result consists of a high-resolution total magnetic anomaly grid. The final magnetic anomaly map was reduced to the pole (RTP), a method that transforms the anomaly as if it has been measured at the magnetic poles, where the geomagnetic field is vertical. The reduction to the pole has the advantage of placing the anomalies over their respective sources (Fig. 4a).

In order to enhance the lateral contrasts and separate shallow from deep sources we applied transformations consisting of: (1) the upward continuation of the magnetic field to 10 km height in order to eliminate short wavelengths associated with shallow sources (Fig. 4b); (2) determination of the first vertical derivative, for identifying regional trends and enhance the shallow sources (Fig. 4c); (3) the analytical signal, to determine the location of sources (Fig. 4d). The latter is based on the square root of the sum of the horizontal and vertical derivatives and thus corresponds to the absolute value of the magnetic anomalies, independent of their magnetization direction. The new magnetic grid of the AMP consist of a higher resolution map than the previous regional map (Correa, 2019) and enables a detailed analysis of the study area.

The 2D forward modeling is based on the method of Talwani (1959). The physical properties (density, magnetic susceptibility and remanence) of the layers used in this study follow values from the literature (Carmichael, 1982) and from basalts of the Abrolhos Archipelago (Ernesto, Personal communication, 2020) and are presented in Table 1. We use susceptibility and remanent magnetization parameters for the igneous rocks since the magnetic anomalies result from the sum of remanent and induced magnetizations. The magnetic remanence contribution of sedimentary and continental basement rocks is usually negligible and was set to zero.

The analysis of magnetic data calibrated by 2D deep seismic crustal sections and well data allowed the association of the different classes of

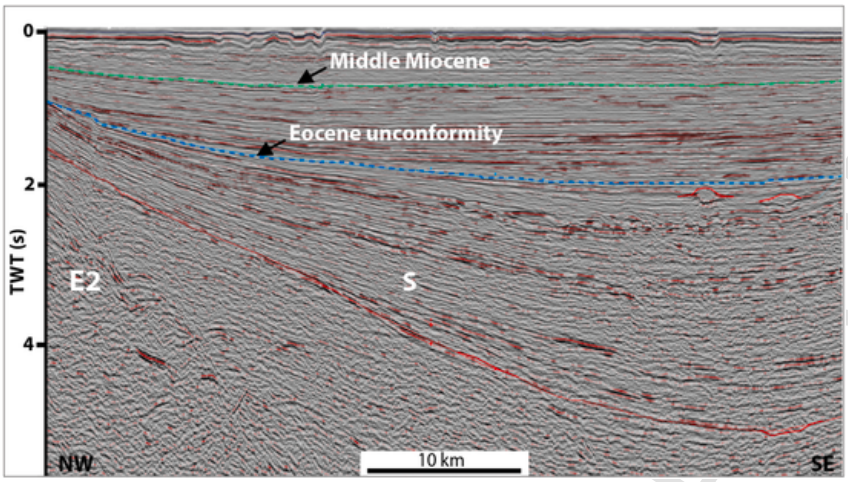


**Fig. 12.** – Seismic section towards the Santa Barbara Island displaying the regional uplift of the area and the upward drag of the pre-Eocene sedimentary sequences. This magmatic edifice is associated with anomaly E2. See location in Fig. 4A.

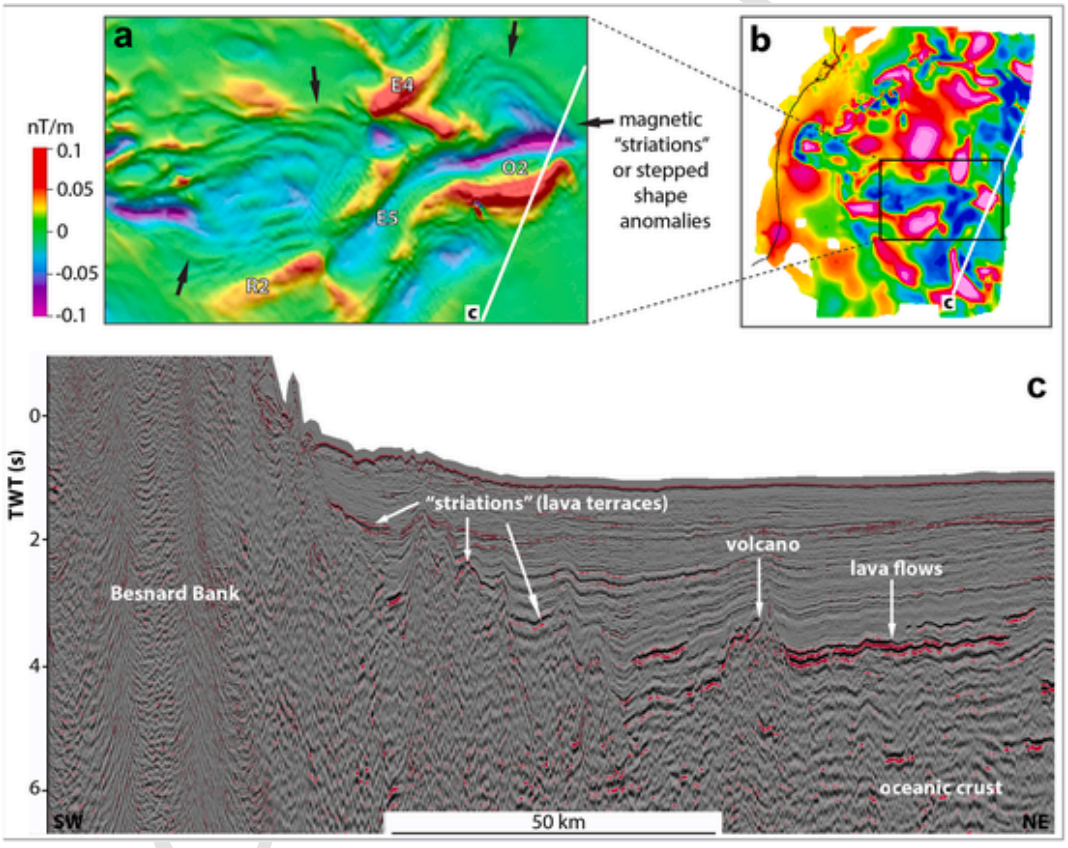


**Fig. 13.** a) Detail of the first derivative of the magnetic anomaly RTP map. b) Magnetic anomaly RTP map of the AMP, with the location of the seismic section. c) Seismic section showing the lava terraces and flows associated with the magnetic "striations" (see text for discussion).

magnetic anomalies (Radial, Elongated and Oceanic) with specific seismofacies. The seismic imaging of the study area was limited due to survey resolution and to the magmatic overprinting that prevented the identification of preexisting structures. Therefore, the seismic interpretation was integrated with magnetic data, which help to constraint the size, vertical extent and differentiate between sedimentary or igneous layers, since the first has no magnetic signature, as well as by 2D forward models at each cross-section, to infer on the composition and crustal structure of the AMP, calibrated by drilling data where available.

## 3. The geophysical characterization of the Abrolhos magmatic province

### 3.1. The spatial arrangement of the igneous edifices

The integration of magnetic and seismic reflexion data provides a 3D view of the AMP. The magnetic anomaly map reduced to the pole (RTP) (Fig. 4a) shows sub-circular and elongated anomalies distributed throughout the Abrolhos Platform (AP) with varying wavelength and amplitude. These magnetic anomalies were classified according to their map-view shape and location as: "Elongated anomalies" (**E1** to **E7**) "Ra-

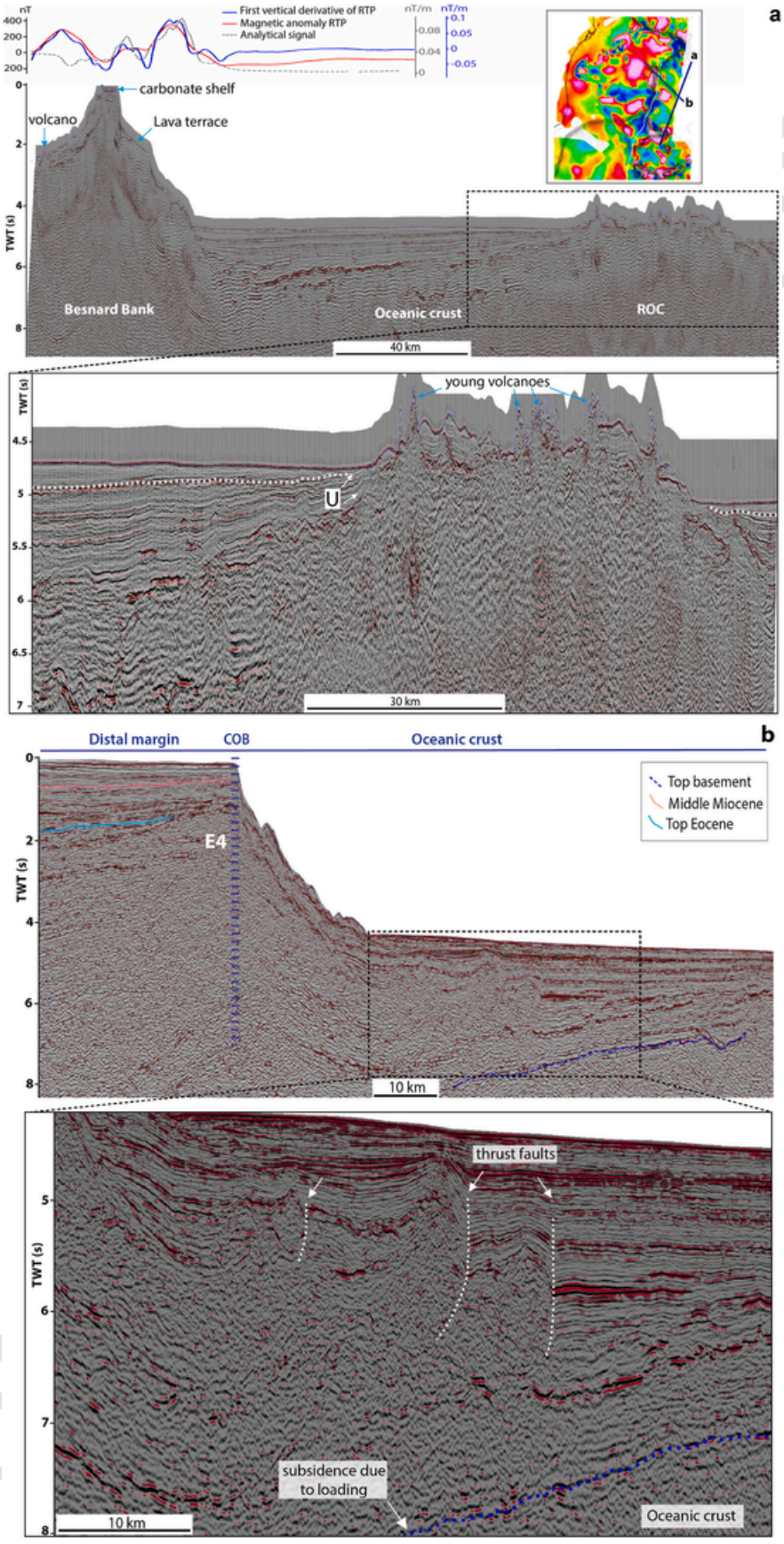
a
First vertical derivative of RTP
Magnetic anomaly RTP
Analytical signal
nT
nT/m
carbonate shelf
volcano
Lava terrace
TWT (s)
Besnard Bank
Oceanic crust
ROC
40 km
young volcanoes
U
30 km
b
Distal margin
COB
Oceanic crust
Top basement
Middle Miocene
Top Eocene
E4
10 km
thrust faults
subsidence due to loading
Oceanic crust

**Fig. 14.** a) Seismic section across the Besnard Bank (BB) and the oceanic crust, with magnetic profiles on top. Note the downward bending of the oceanic crust near the BB and the Recent Oceanic Complex (ROC at the zoom section), where young volcanoes uplift post-Eocene strata and impinge onto the seafloor; b) Seismic section showing thrust faults and flexural loading of the oceanic crust.

dial anomalies" (**R1** and **R2**), and "Oceanic anomalies" (**O1** and **O2**). A detailed description of the individual anomalies is presented at Table 2.

At the central part of the Abrolhos Platform (AP), a pronounced magnetic high R1 (~400 nT) with intermediate wavelength (~40 km) is present (Fig. 4a). The **R1** is observed at the upward continued map that reflects long-wavelength sources (Fig. 4b) but its signature is subdued on the first derivative map, related to higher frequency sources. (Fig. 4c). These characteristics indicate that **R1** is associated with intermediate and deep (>5 kms below sea level) magnetic sources. It is surrounded by smaller magnetic anomalies (ca. 15 kms width) of high amplitude (~300–400 nT), named **E1** to **E4**. The central **R1** widens and displays lateral prolongations towards adjacent **E** anomalies at the upward continued map (Fig. 4b), what suggests that this large and deep magnetic center may be connected with adjacent smaller magnetic sources, forming lateral "ramifications". In the southern AMP the most prominent anomaly observed is **R2**. This anomaly also exhibits lateral prolongations towards the surrounding smaller anomalies **E5, E6**, and **E7**, as observed in Fig. 4b. The **E** anomalies have expression on both long- and short-wavelength magnetic maps (Fig. 4b and c, respectively), indicating that they are associated with superficial and deep-seated sources (see Table 2 for details).

The spatial distribution of the individual magnetic sources at the AMP shows preferred orientations of the **E** anomalies, that trend NW-SE, NNE-SSW and NE-SW (Figs. 2, 4a and 4c). The outer limits of the AMP seem to follow regional lineaments oriented NW-SE and NE-SW. These orientations are parallel to the border of the São Francisco Craton, the Paramirim aulacogen and the rift transfer zones (NW-SE), and to the Cretaceous faults and the Ribeira orogeny (NE-SW), respectively (Figs. 2 and 5).

It is also possible to observe that the general arrangement of the magnetic anomalies at the AMP exhibit a systematic geometric disposition of the **R** relative to the **E** anomalies (Figs. 4a and 5). The central large **R** anomalies are radially surrounded by smaller "satellite" **E** anomalies. These "satellite" anomalies are disposed at approximately high angles relative to those centers (>90°). For instance, the **R1** anomaly is surrounded to the east by the NE-SW trending **E2**, to the north by the NW-SE trending **E3** and to the west by the NE-SW trending **E4**.

### 3.2. The morphostructure of the AMP: seismic and magnetic observations

The pronounced "Radial anomalies" **R1** and **R2** (Fig. 4) are associated with a reflection-free seismofacies that passes laterally into more reflective seismofacies with parallel/subparallel and divergent reflection configurations interpreted as sedimentary rocks (Figs. 5–10). However, there is no clear, continuous seismic reflector representing the transition from igneous to sedimentary rocks. Their contact is usually gradual and characterized by lateral sediment-volcanic interfingering seismofacies (Fig. 10). The morphology from seismic data of **R1** and **R2** suggests continuous igneous bodies extending from deep to shallow depths (between 5 and 1 s TWT, respectively), in agreement with their subdued magnetic signature on the first derivative map (related to shallow seated sources), and on the upward continuation map (related to deep seated sources) (Fig. 4c and b, respectively). The igneous rocks associated with anomaly **R1** have been drilled by well 1ESS20 (Figs. 3f and 4).

The igneous edifices associated with the **E** anomalies are located at the outer border of the AMP, characterized by massive seismofacies that extend vertically for ~2–4 s (TWT). These are emplaced within parallel to subparallel high reflective seismofacies indicative of sedimentary rocks. The **E** igneous edifices exhibit tabular and conical shapes. For example, a tabular sub-horizontal shape is be observed for **E4** (Fig. 6) and **E7** (Figs. 8 and 11a), a tabular inclined shape for **E6** (Fig. 10) and a conical shape for **E5** (Figs. 9 and 11c). Anomaly **E7** is associated in seismic section with two shallow bodies of massive texture emplaced within sedimentary rocks and is dissected by a fault (Fig. 11a). The peaks on the first derivative of the RTP map associated with igneous body **E7** (Fig. 4c and the profile of Fig. 8) suggests a shallow magmatic emplacement, confirmed by the well 1ESS4 (Fig. 3f). **E3** exhibits a tabular morphology and reflective seismofacies suggesting intercalation of igneous and sedimentary rock layers (Fig. 8). The elongated anomaly **E2** (Fig. 4) correlates with an igneous body that exibits a normal drag of host rock at flanks and a drape fold of the Eocene and younger sediments on top (Fig. 12), indicating uplift of the pre-Eocene sequences. This uplift resulted in deep-water sediments, diabases and basalt at the Abrolhos Archipelago (well 2SBST1) outcropping at the Santa Barbara Island (Fig. 3f). A detail seismic section shows a high angle discordant reflector interpreted as a possible dike feeding a volcanic cone (Fig. 11d). Additionally, sills of basalts intrude Late Cretaceous to Eocene sedimentary sequences in Santa Barbara Island (Fig. 3d).

The regional disposition of the **E** anomalies surrounding the central **R** anomalies form the outer borders of the AMP, with amplitudes of ~250–350 nT (Fig. 4). Their wavelength difference and seismic signature suggest that the first corresponds to shallower seated igneous edifices in comparison with the deeper and central ones (Figs. 6–9) (see Table 2 for a detailed description of each anomaly). This is supported by our 2D forward modeling (Figs. 6–9) which shows that the sources for the E anomalies are consistent with shallower seated bodies, while R anomalies require deeper and larger sources, extending vertically down to near the top of the basement.

### 3.3. The extent of the AMP

The analytical signal (AS) map (Fig. 4d) represents all existing magnetic sources (positive and negative) within the AMP. On this map, some areas showing negative signature at the RTP map correspond to high gradients (Fig. 4a and d, respectively). On all profiles (Figs. 6–9) it is possible to observe several igneous bodies identified in seismic data displaying both normal and reverse magnetic anomalies (indicated as "Normal M" and "Reverse M″ at the magnetic profiles, see also Table 2). For example, the igneous edifices related to the **E7** and **E3** anomalies displays negative and positive high amplitude values (Fig. 4a and magnetic profile of Fig. 8) that correspond to high gradients at the AS map (Fig. 4d). The paleomagnetic data from basalts of the Abrolhos Archipelago indicates the existence of positive and negative remanent magnetization on the volcanic rocks of the AMP (Montes-Lauar, 1993; Ernesto, Personal communication). These observations indicate that the **E7** and **E3** comprise igneous edifices formed by different magmatic pulses during which the geomagnetic field of the Earth changed its polarity. That imprinted a normal magnetization and later a reverse magnetization direction (or vice-versa) during the formation of those igneous edifices. This is consistent with the long duration of the magmatism of this magmatic province.

Based on the AS anomalies we mapped the extent of all magnetic sources at the AMP (Fig. 4d), resulting in an estimated area of ~63,000 km$^2$. It shows that the AMP extends beyond the Abrolhos Platform, and includes the Besnard Bank and distal recent oceanic volcanic complexes, here referred as ROC (Fig. 9).

The identification of the COB in the AMP was speculative since the deep crustal structure imaging from seismic data was affected by the widespread Abrolhos volcanism. Thus, we have defined the COB at the landward limit of the first undisputable oceanic crust, in general located at the edge of the Abrolhos Platform (Fig. 4). The oceanward limit

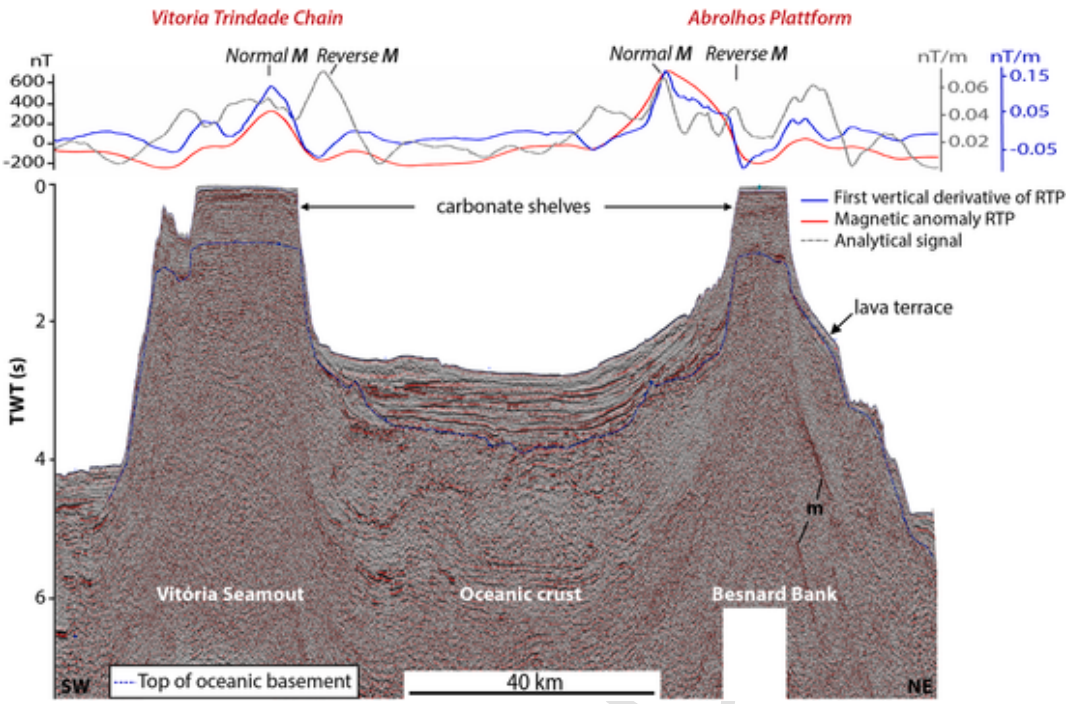


**Fig. 15.** a) Seismic section across the Besnard Bank and the Vitória-Trindade seamounts, with magnetic profiles on top. See location in Fig. 4A.

of the AMP does not show a correlation with the COB (Fig. 4d), extending onto oceanic crust and forming two groups of anomalies: **O1** and **O2**, which display the highest amplitudes of the AMP (see Table 2). In seismic sections these are associated with buried igneous bodies of conical shapes, flat top guyots and recent volcanic cone morphologies (Figs. 6, 9 and 13). It is possible to observe a pattern of subtle curvilinear "striations" encircling **R2, O1** and **O2** anomalies (Fig. 13a). Its shape and reflection pattern in seismic data resemble those of lava terraces and/or igneous sills, with a "stepped" shape in map-view. These magnetic "striations" show concordant and discordant high amplitude reflectors at different stratigraphic intervals. (Fig. 13c).

### *3.4. The tectono-stratigraphy of the AMP volcanic edifices*

The observation of a high angle truncation of the Lower Eocene layers (and older units) and onlapping reflectors of younger carbonate sequences indicate that the AMP emplacement affected the pre-Eocene deposits (Fig. 10). There are evidences of remobilization of salt towards the south and the north of the Mucuri Basin (Figs. 5 and 11a), and gravity sliding of sediments and thrusts structures seawards from the continental shelf edge (Fig. 14b), suggesting a regional uplift. A pronounced downward bending of the first oceanic crust (Fig. 14) and upward seismic reflectors at ~6 s (TWT) are observed at the COB. The2D forward models (Figs. 6–9) also indicate the flexural loading of the oceanic crust at the COB.

More than 70 vents were identified in this study, mainly concentrated along the eastern border of the Abrolhos Carbonate Platform (Fig. 16). The vent structures display convex (upper) and concave (lower) boundaries on seismic sections, disturbing the lateral continuity of the seismic reflectors and producing a vertical zone of chaotic reflections (Figs. 6–11). They display ~2 km of mean width and affect the sedimentary sequences from the Eocene Unconformity up to the Middle Miocene unconformity. A stratigraphic relationship between the vents and the volcanic edifices **R1**, **R2, E3, E4**, and **E5** (Figs. 6–10) was observed, and of some vents are associated with magnetic highs. None of these vents have been drilled. The lack of rocks with high amounts of organic carbon in the sedimentary section and the absence of hydrocarbon generation in this part of the basin do not support an origin from organic matter degradation (e.g. gas chimneys). Possible hypothesis about the nature of these vents are discussed in section 4.3.

## 4. Discussion

The magnetic, seismic and well analyses revealed the presence of intrusive and extrusive igneous rocks throughout the AMP, which extends beyond the limits of the Abrolhos Carbonate Platform (AP). With the objective of investigating the morphostructure, spatial distribution, and the impact of the AMP on the Brazilian margin, we present a discussion about its emplacement, the possible structural controls, basin modifications and timing.

From our quantitative and qualitative analyses, three important points become evident: 1) The great volume of the Abrolhos magmatism (Fig. 17), equivalent to other oceanic volcanic provinces like the Canary and Marquesas archipelagos (Miller et al., 2015; Konrad et al., 2018); 2) the magmatism affected not only the continental lithosphere but also extended onto oceanic crust as post-formation within plate volcanic complexes (Recent Oceanic Complex – ROC, Figs. 1, 7 and 94a); 3) the magmatic structures pull up the pre-Eocene strata impinging at the ocean floor and result in regional uplift. The implications of these observations will be discussed in the next sections.

### *4.1. The emplacement of the Abrolhos Magmatic Province*

The areal emplacement of the AMP revealed a systematic pattern based on the magnetic anomaly maps (Fig. 4). The largest bodies (**R1** and **R2**) are located at the center and are laterally connected to several surrounding smaller igneous edifices (**E** or "satellite" anomalies). The **E** anomalies are in general systematically disposed at high angles (>90°) relative to the **R** anomalies, forming a network of small (~5–7 km wavelength), intermediate (~15–20 km wavelength) and large igneous edifices (>25 km wavelength). The central edifices **R** correspond in seismic data to thick igneous bodies, emplaced from deep (>5 km) to shallow depths (~2 km) (Figs. 6–10), while the outer **E** edifices are shallower (<1 km), smaller in size and vertical extent (Fig. 11). All these igneous edifices intruded the continental crustal basement, the oceanic crust, and the Pre-Eocene sedimentary sequences (Figs. 6–9).

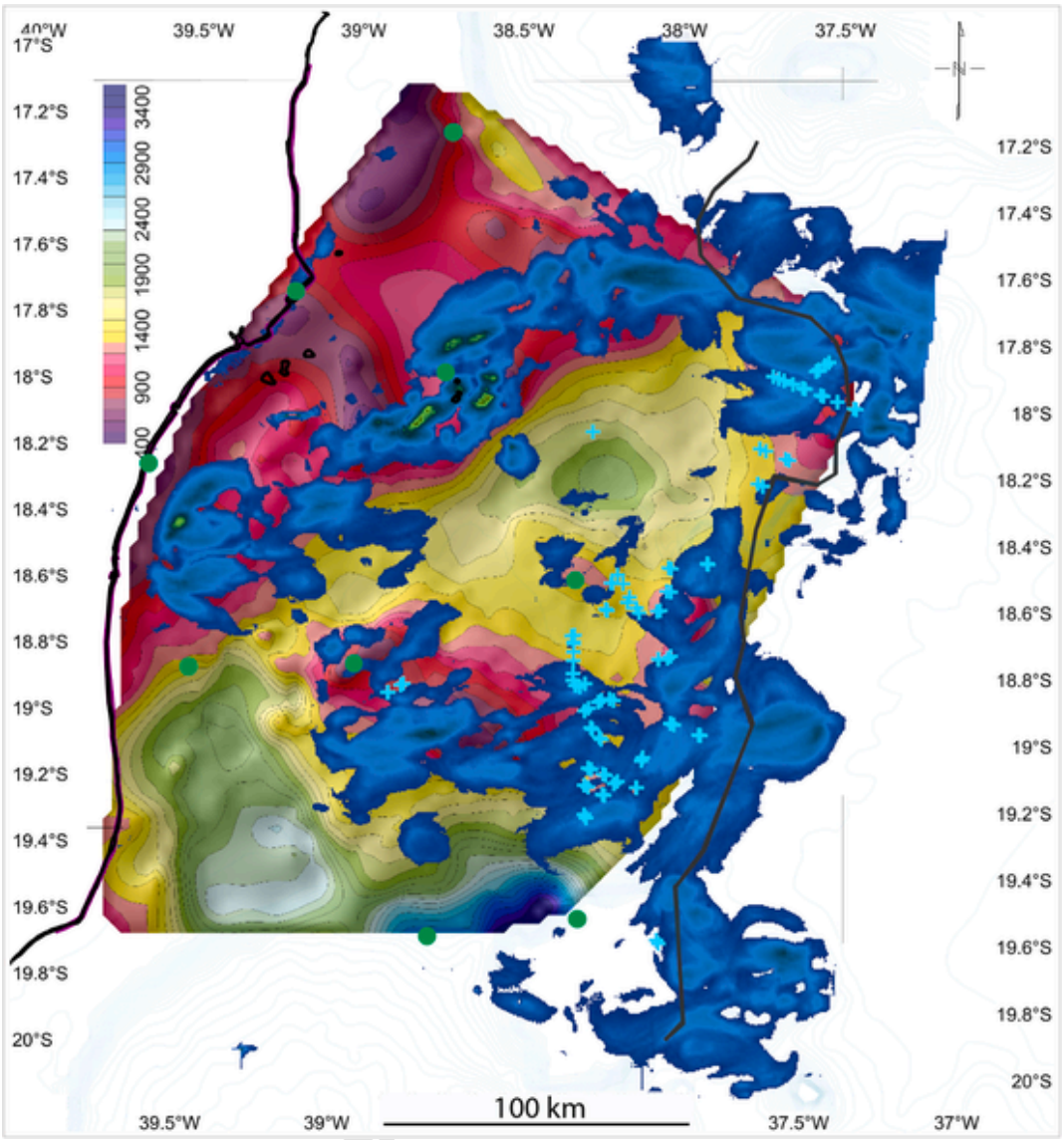


**Fig. 16.** Composite map of the time structure of the Top Eocene horizon, overlain by the analytical signal anomalies (blue contours). Light blue crosses are mapped vents and green circles are wells with AMP basalts. (For interpretation of the references to color in this figure legend, the reader is referred to the Web version of this article.)

From the spatial arrangement of the igneous edifices at the AMP (Figs. 4 and 6 to 9), it is likely that the central sources correspond to the main magma storage locations, represented by **R1** and **R2**, which connect to distal eruptive centers identified as anomalies **E1** to **E7**. Such radiating formation (Fig. 5) show a geometry similar to that observed in the active rift arms of triple junction (Sengor and Burke, 1978). In these settings, magma flow creates radiating volcanic ridges, similar to Hawaiian seamounts and El Hierro on the Canary Islands (Mitchel, 2001). The morphology of the magmatic structures observed in this study frequently display a stellate shape in map view (Fig. 5), whose origin might be associated with further growth of initial magma bodies, leading to more complex structures by additional supply of magma with time (Mitchell, 2001).

We have mapped igneous intrusives and edifices of different shapes including dykes and sills (Figs. 11 and 13), probably related to the AMP plumbing system. Although our seismic data resolution is unsufficient to resolve the deep crustal structures, analogs of plumbing system globally may provide valuable insights to understand the AMP emplacement mechanism. For instance, Magee et al. (2019) and references therein show that plumbing systems vary with depth: at shallow levels (<3 km depth) the system may consist of extensive sill complexes. Thus, magma can be transported laterally, feeding eruption sites that are hundreds of kilometers from their original melt sources by sills and dikes, though dykes form over a wide range of depths (from hundreds of meters to several tens of kilometers) according to Jerram and Bryan (2015). Recent studies propose that mafic sills and inclined sheets form interconnected networks of magma transport, distributing melt at distances of 12 km vertically and 4100 km laterally (Cartwright and Hansen, 2006; Leat, 2008). Such network could feed distant volcanic eruptions from the mantle source (Magee, 2019, after Magee et al., 2013; Muirhead et al., 2014; Jerram and Bryan, 2015). Similar regional distribution was reported by Pinel and Jaupart (2004), with the volcanic provinces at the central area corresponding to the feeding sources for the surrounding bodies.

We propose for the AMP area a 3D magmatic system represented schematically at Fig. 18. The conceptual plumbing system displays a major magmatic center connected to the mantle through a wide feeding system. Magma may be distributed vertically by dyke-like structures and laterally by sill-like structures and be stored at different crustal levels, replenished by successive volcanic events. This conceptual system

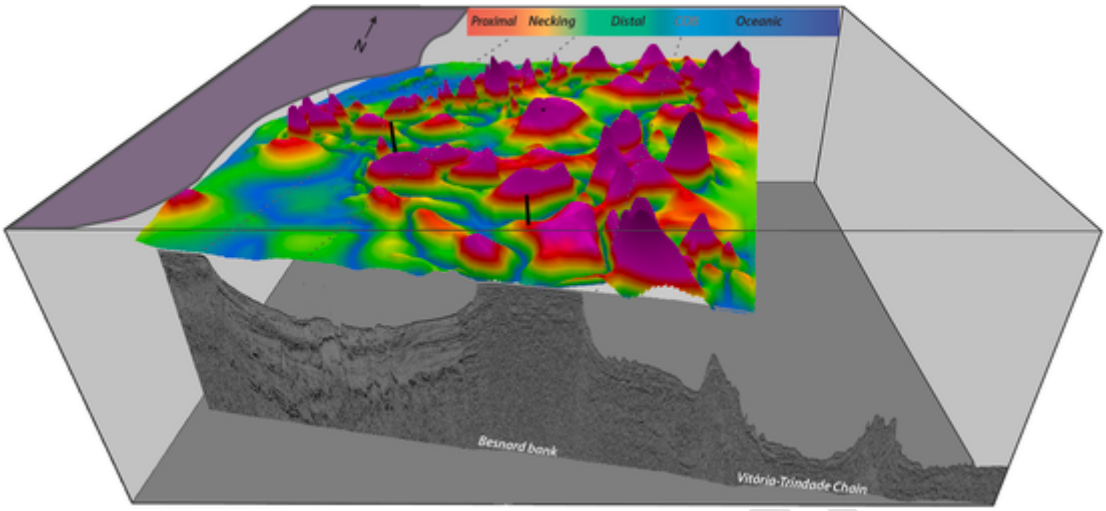


**Fig. 17.** Block diagram showing the distribution of igneous edifices in the AMP (based on magnetic anomalies and seismic interpretation), overlying a seismic section crossing the Besnard Bank (southern AMP) and the nearby seamounts of the VTC. The margin domains (proximal, necking, distal, COB and oceanic, see Stanton et al., 2016 for definitions) boundaries are projected across the AMP as thin dashed lines.

is in agreement with that proposed by Jerram and Bryan (2015) and supported by the age, paleomagnetic data and geochemical modeling of trace and isotopes elements (Arena, 2008) of the Abrolhos basalts.

Our proposed model is based in previous works and on our geophysical data. However, our interpretations are limited due to several factors: 1) The original rifted margin was overprinted by widespread intrusives and extrusives that mask the preexisting structures (Fig. 17); 2) the data resolution is insufficient to image deeper structures or variations in seismic reflective strength at depth, which would indicate differing degrees of intrusion between the ductile lower crust and upper crust and related magmatic plumbing system; 3) it is in general difficult to fully image the characteristics of magmatic plumbing systems by seismic, as pointed out by Schofield et al. (2017a,b).

### 4.2. The structural control to the emplacement of the AMP

The E magnetic anomalies of the outer borders of the AMP follow two preferred orientations: NE-SW and NW-SE. These trends are subparallel to preexisting crustal structures like the Araçuaí Belt, the Paramirim aulacogen, the border of the São Francisco craton and rift transfer zones, and to the Ribeira Belt and Cretaceous rift-related faults (Figs. 2 and 5), respectively. Oceanwards the spatial distribution of igneous edifices extend beyond the COB (ROC at Fig. 14), with flexural loading of the oceanic crust (Fig. 14) probably associated with the emplacement of the volcanic edifices. Additionally, near the COB a large concentration of vents is observed (Fig. 16).

As showed in previous studies globally, magmatic emplacements commonly follow lateral variations of crustal thickness, which are frequent pathways that control igneous intrusions (Jourdan et al., 2006). The magmatism may be focused at reactivated faults, specially transtensional structures, as observed at the North Sea basins (Blazic and Moreau, 2016), the Campos Basin (Oreiro et al., 2008) and the African intracratonic basin (Moreau et al., 1994). At the Voring margin, Planke et al. (2005) identified an extensive sill complex and proposed that melt was emplaced along weakness zones.

It is reasonable to believe that the Eocene magmatism would utilise from preexisting fractures and faults of the Brazilian rifted margin and continental lithosphere. The compositional boundary of the COB may have acted as a weakness zone favoring the recent volcanic activity observed at the eastward part of the AMP. Thus, the observations presented here appear to indicate that the emplacement of the AMP has (at least partially) being influenced by inherited crustal/lithospheric discontinuities (crustal weakness zones), associated with Precambrian and/or Cretaceous breakup structures.

### 4.3. How did the AMP influence the post-rift tectono-sedimentary evolution of the Eastern Brazilian margin (Espírito Santo and Mucuri basins)?

A tectonostratigraphic relationship between the Abrolhos magmatic structures and the pre-Eocene sedimentary sequences is observed in the present study. The direct correlation between the high gradients at analytical signal of the magnetic anomalies (blue regions) and variations of the Top Eocene unconformity (in time, Fig. 16) brings to notice that the spatial distribution of the shallower igneous edifices, mainly concentrated at the outer borders of the AMP, coincides with Eocene structural highs. The central and structurally lower part of the AMP is constituted by deeper-seated igneous edifices, characterizing larger accommodation space and differential subsidence and compaction (Figs. 8 and 17). The 3D magnetic model overlying the seismic section of Fig. 17 illustrates the modification of the original margin stratigraphy due to the AMP emplacement. It shows a normal dipping-to-the-basin physiography interrupted and uplifted by the igneous intrusions at the Besnard Bank. On top, the magnetic map represents all sources (hot colors) at the study area and show the widespread occurrence of the igneous edifices of the AMP.

Additionally, the emplacement of the AMP uplifted the deep-water Cretaceous sediments, exposed at the Abrolhos Archipelago, remobilized the salt deposits and generated compressive structures (Fig. 14b) and syn-tectonic wedges of sediments and volcaniclastic rocks around the main magmatic edifices. Similar interpretations have been reported previously by Mohriak (2005) and Sobreira and França (2006) and are sustained by apatite fission-track data that indicate a maximum uplift at ~50 Ma (Mohriak, 2005). This uplift resulted in the development of a shallow-water (<100 m depth) carbonate platform in previous areas of ultra-deep water, which remains until present (Fig. 16b). Therefore the tectonic and depositional changes created by the AMP emplacement profoundly modified the original Mucuri basin stratigraphy.

### 4.4. Evidences of a long-lived and widespread intraplate magmatism

At the AMP the geochronological data (Fig. 3) indicate Paleogene ages for the igneous rocks. However, there is a discrepancy between these ages and the tectonostratigraphic relationships between the vents and hosting sedimentary rocks, since the vents disrupt the overlying deposits up to the Miocene unconformity, indicating a Middle Miocene

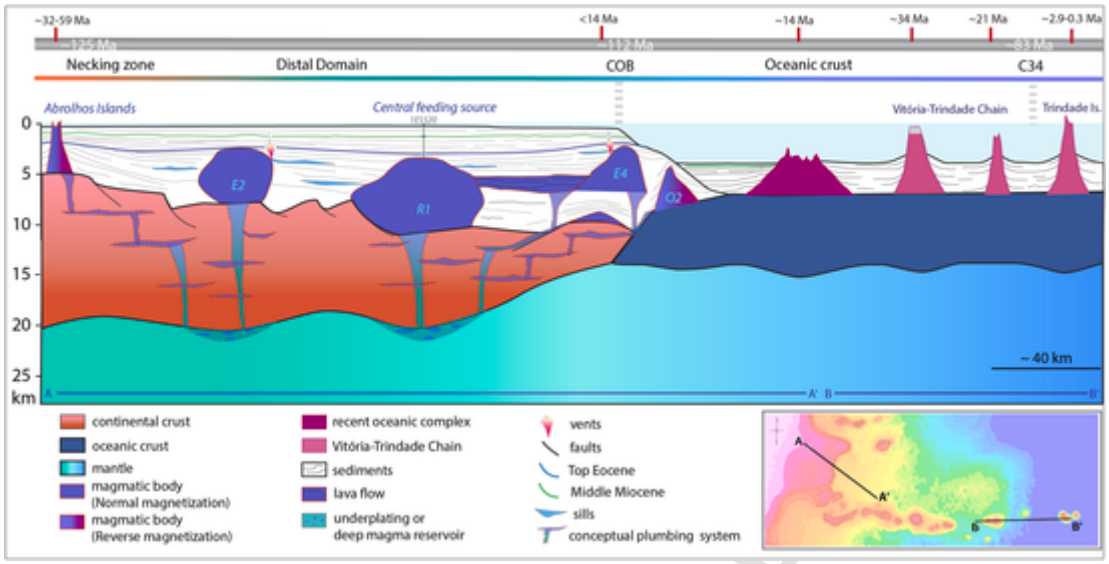


**Fig. 18.** Composite geological cross-section idealized for the AMP, showing the spatial relationships of the igneous edifices and their continuation along the Vitória-Trindade Chain. A conceptual plumbing system is proposed, based on the works of Magee et al. (2019), Forni et al. (2018) and Jerram and Bryan (2015). The location of the 2 sections A-A′ and B–B′ that compose the cross-section is shown on the bathymetric map below the section.

age (Fig. 10). Equivalent magmatic ages are reported at the Dogaressa seamount (VTC) located 650 km to the east of the AMP (Fig. 1). As the vents are often observed on the surface or lateral walls of igneous edifices and some are coincident with high amplitude magnetic anomalies (Figs. 6–9), we propose that they correspond to fluids/volcanic gases related to the intrusion of sills or the igneous edifices.

Similar observations are recognized from basins worldwide that were affected by large igneous events, such as the North Atlantic margins (Hansen et al., 2006) or the Karoo Basin in South Africa (Svensen et al., 2006). In the Karoo Basin, the hydrothermal vents display widths of hundreds of meters and pre-date the main magmatic event (Svensen et al., 2006). In the Voring and More basins they are crater-, dome- or eye-shaped and connected to sills, vary from 1 to 5 kms width and originated from a Paleocene intrusive event (Svensen et al., 2004; Planke et al., 2005). In the Senegal Basin, the hydrothermal vents and intrusion related folds are associated with igneous sills, which origin is related to a widespread Miocene igneous event that led to vertical magma migration along re-activated basement structures (Hansen et al., 2008).

The tectonostratigraphic observations that indicate the presence of hydrothermal vents at the AMP extend the igneous activity in this region into the Middle Miocene, implying a duration of ~56 Myr for AMP magmatism. In agreement with this, the magnetic analysis revealed the presence of magmatic sources characterized by negative and positive magnetic anomalies (see the RTP maps of Fig. 4), all corresponding to high amplitudes in the analytical signal map. That indicates existing sources with normal magnetization direction and others with reverse magnetization direction at the AMP, with some volcanic structures apparently carrying both within one single morphostructure, like the Besnard Bank and the Vitória Seamount (Fig. 15). These observations are supported by paleomagnetic data (Ernesto, Personal communication, 2020) of Abrolhos basalts, which report normal and reverse remnant magnetization directions for samples collected at closely located islands. These evidences indicate multiple-stage intrusions at the AMP, from Eocene to Middle Miocene.

In addition, the magnetic anomaly and seismic pattern observed on the Besnard Bank, at the southern part of the AMP, display analogies with those on the Vitória Seamount, in the VTC (Figs. 1 and 4). These structures display similar characteristics like height, thickness of carbonate shelf and seismofacies (Fig. 15), as well as magnetic anomalies wavelength and amplitude. The comparable thickness of their carbonate shelves, which result from crustal subsidence and depositional rates, suggesting a similar evolution. The presence of such a wide and shallow carbonate shelf at the AMP also indicates that the igneous edifices did not substantially subside since the Eocene and suggest a stable thermal structure for this region.

Therefore, the tectono-stratigraphy and magnetic data provide evidence for long-term and persistent magmatic activity in the AMP area, and connect the volcanism of the AMP with that of the VTC (see Fig. 17), recently active in the Trindade Island (Pires et al., 2016).

### 4.5. *Possible origins of the AMP*

The morphostructure, spatial arrangement, ages and magnetic data indicate that the AMP region underwent continuous and long-lived magmatic activity since 56 Ma and extending laterally over 1000 km. The presence of hydrothermal vents in the AMP affecting sediments as recent as Middle Miocene and contemporary magmatic activity at the Dogaressa seamount (Fig. 1), suggests a wide magmatically active region, where the magmatic activity first created a diffuse and widespread magmatic complex and later a linear volcanic chain active up to the present day.

From the S-wave velocity tomographic models of the upper mantle (model A2019 of Celli et al., 2019), lower seismic velocities down to 260 km depth are observed in the region of the AMP and VTC, indicating a hotter mantle. Such low-velocity regions may act as active mantle upwelling areas at present-day (Celli et al., 2020 and references therein). This region also corresponds to an anomalous positive dynamic topography (Cowie and Kusznir, 2018), indicating a hot mantle thermal structure or upwelling convection. These could explain the long-duration of the magmatism and the formation and maintenance of the present-day shallow carbonate shelf.

The size and extent of the AMP and its proximity to the VTC led several authors to suggest the influence of a hotspot (Thompson et al., 1989; Gibson et al., 1995; Siebel et al., 2000). Nevertheless, the Abrolhos magmatism does not show an age progression from west to east as expected from a classical hotspot mechanism where the plume is fixed in the mantle reference frame (e.g. Hawaii). The timing, spatial extent and duration of AMP magmatic activity are inconsistent with a simple linear hotspot trail.

The closest analog to the Abrolhos province would be the Canary Islands, where the temporal and spatial distribution of seamounts are incompatible with single fixed-plume models (Van Den Bogaard, 2013).

Mechanisms such as shallow mantle convection at the rifted continental lithosphere flanks or the combinations of passive mantle and plate-related convection have been invoked to explain the seamounts age distribution of the Canary Islands (Van Den Bogaard, 2013 and references therein).

## 5. Conclusions

We present a detailed mapping of the Abrolhos Magmatic Province (AMP) and show that it consists of an assembly of large volcanic edifices, each with individual diameters in excess of 50 km (~600–2100 km$^2$) and each formed by multiple volcanic events, as recorded by magnetic anomalies and paleomagnetic data. Observed magnetic anomalies require that there are both shallow and deep seated volcanoes emplaced in continental and oceanic lithosphere.

The systematic spatial arrangement of the AMP structures reveals a stellate pattern, with larger magmatic bodies located at the central Abrolhos Platform and at greater depths. These may constitute the main feeding source for the shallower igneous edifices located at the borders. The emplacement of the AMP appears to follow preexisting structural trends like Precambrian continental structures and Cretaceous margin faults, suggesting that it may have been partially controlled by inheritance.

The emplacement of the AMP had a profound impact on the tectonosedimentary evolution of the Brazilian margin. It disturbed the previous Cretaceous margin sedimentary basin and continental crust, leading to differential post-rift erosional and depositional responses, and altered the vertical isostatic balance of the margin. Additionally, the igneous structural highs and lows created the framework for sedimentation and formation of a shallow carbonate platform since Eocene to present.

We interpret vents imaged on reflection seismic and coincident with high amplitude magnetic anomalies as hydrothermal vents. They suggest magmatic activity continuing into the Neogene. Equivalent magmatic ages are observed at the Vitoria-Trindade Chain 650 km to the east of the AMP, indicating widespread simultaneous magmatism. Our observations integrated with previous mantle velocity and dynamic models suggest that the AMP and VTC originated over a region of anomalous mantle thermal structure. Nevertheless, the timing, duration and spatial distribution of AMP magmatism are inconsistent with a fixed hotspot in the mantle reference frame, requiring an alternative mechanism like non-stationary, migrating hotspot or plate-related convection, hypotheses that may be explored in future studies.

## Credit statement

Natasha Stanton: Conceptualization, Methodology, Writing, Magnetic Analysis. Andres C. Gordon: Conceptualization, Writing, Seismic Analysis. Nick Kusznir: Conceptualization, Investigation, Reviewing. Cassia Cardozo: Investigation, Seismic Analysis.

## Uncited references

; ; ; ; ; ; ; ; .

## Declaration of competing interest

The authors declare that they have no known competing financial interests or personal relationships that could have appeared to influence the work reported in this paper.

## Aknowledgments

We would like to thank CAPES (Coordenação de Aperfeiçoamento de Pessoal de Nível Superior) for Cassia Cardozo's scholarship and to ANP for the dataset. The authors are grateful to the reviewers for their useful comments that improved the paper.

## References

Alkmim, F.F., Marshak, S., Pedrosa-Soares, A.C., Peres, G.G., Cruz, S.C.P., Whittington, A., 2006. Kinematic evolution of the Araçuaí-West Congo orogen in Brazil and Africa: nutcracker tectonics during the Neoproterozoic assembly of Gondwana. Precambrian Res. 149, 43–64. https://doi.org/10.1016/j.precamres.2006.06.007.

Alkmim, F.F., Kuchenbecker, M., Reis, H.L.S., Pedrosa-Soares, A.C., 2017. The Araçuai belt. In: Heilbron, M. (Ed.), São Francisco Craton, Eastern Brazil, Regional Geology Reviews. Springer International Publishing, pp. 255–276.

Almeida, F.F.M., 1961. Geologia e petrologia da Ilha Trindade. DNPM-DGM, p. 168.

Almeida, F.F.M., 1973. The precambrian evolution of the south American cratonic margin. South of Amazon river. In: Nairn and Stelli (Ed.), The Ocean Basin and Margins, vol. 1. Plenun, Nova York, pp. 411–416.

Almeida, F.M., F., 2006. Ilhas Oceânicas Brasileiras E Suas Relações Com a Tectônica Atlântica. Terrae Didatica 2, 3–18.

Almeida, F.F.M., Carneiro, C.D.R., Mizusaki, A.M.P., 1996. Correlação do magmatismo das bacias da margem continental Brasileira com o das áreas emersas adjacentes. Rev. Bras. Geociencias 26 (3), 125–138.

Alves, E.C., Maia, M., Sichel, S.E., Campos, C.M.P., 2006. Zona de Fratura de Vitória-trindade no Atlântico Sudeste e suas implicações tectônicas. Rev. Bras. Geofís. 24 (1), 117–127.

Arena, M.C., 2008. Petrologia da sucessão magmática do arquipélago de Abrolhos: Master Thesis. Universidade do Estado do Rio de Janeiro.

Assumpçao, M., Bianchi, M.A.M., França, G.S.L., Rocha, M., Barbosa, J.R., 2004. Seismic studies of the Brasília fold belt at the western border of the São Francisco Craton, Central Brazil, using receiver function, surface-wave dispersion and teleseismic. Tectonophysics 388 (1–4), 173–185. https://doi.org/10.1016/j.tecto.2004.04.029.

Bauer, K., Trumbull, R.B., Vietor, T., 2003. Geophysical images and a crustal model of intrusive structures beneath the Messum ring complex, Namibia. Earth Planet Sci. Lett. 216 (1), 65–80. https://doi.org/10.1016/S0012-821X(03)00486-2.

Bento dos Santos, T.M., Tassinari, C.C.G., Fonseca, P.E., 2015. Diachronic collision, slab break-off and long-term high thermal flux in the Brasiliano–Pan-African orogeny: implications for the geodynamic evolution of the Mantiqueira Province. Precambrian Res. 260, 1–22.

Blaich, O.A., Faleide, J.I., Tsikalas, F., 2011. Crustal breakup and continenteocean transition at South Atlantic conjugate margins. J. Geophys. Res. 116.

Blažić, L., Moreau, J., 2017. Discovery of Lower Cretaceous hydrothermal vent complexes in a late rifting setting, southern North Sea: insights from 3D imaging. Journal of the Geological Society 174, 233–241. https://doi.org/https://.org/10.1144/jgs2015-155.

Bulhões, E.M., De Amorim, W.N., 2005. Princípio da SismoCamada Elementar e sua aplicação à Técnica Volume de Amplitudes (tecVA). In: 9th International Congress of the Brazilian Geophysical Society. European Association of Geoscientists & Engineers.

Cainelli, C., Mohriak, W.U., 1999. Some remarks on the evolution of sedimentary basins along the Eastern Brazilian continental margin. Episodes 22, 206 216.

Cande, S.C., Labrecque, J.L., e Haxby, W.F., 1988. Plate kinematics of the South Atlantic: chron 34 to present. J. Geophys. Res. 93 (13), 13–492 497.

Cardozo, C.L.A., 2018. Província Magmática de Abrolhos e sua influência na evolução pós-rifte da margem leste brasileira. University of Rio de Janeiro State, p. 90p Master thesis.

Carmichael, R.S., 1982. Magnetic properties of minerals and rocks. In: Carmichael, R.S. (Ed.), Handbook of Physical Properties of Rocks, Volume II. CRC Press, Boca Raton, p. 345.

Cartwright, J., Hansen, D.M., 2006. Magma transport through the crust via interconnected sill complexes. Geology 34, 929–932.

Cavalcante, C.H., Fossen, R.P., De Almeida, M.H.B.M., Hollanda, M., Silva, E., 2019. Reviewing the puzzling intracontinental termination of the Araçuaí-West Congo orogenic belt and its implications for orogenic development. Precambrian Res. 322, 85–98. https://doi.org/10.1016/j.precamres.2018.12.025.

Celli, N.L., Lebedev, S., Schaeffer, A.J., Ravenna, M., Gaina, C., 2020. The upper mantle beneath the South Atlantic Ocean, South America and Africa from waveform tomography with massive data sets. Geophys. J. Int. 221 (1), 178–204.

Chang, H.K., Kowsmann, R.O., Figueiredo, A.M.F., Bender, A.A., 1992. Tectonics and stratigraphy of the East Brazil rift system (EBRIS): an overview. Tectonophysics 213, 97–138.

Cordani, U.G., 1970. Idade do vulcanismo no oceano Atlântico sul. Boletim IGA 1, 9–75.

Correa, R.T., 2019. Mapa da anomalia magnética do Brasil (terceira edição). Escala 1:5. 000.000. Brasília, SGB-CPRM – Serviço Geológico do Brasil.

Cowie, L., Kusznir, N., 2018. Renormalisation of global mantle dynamic topography predictions using residual topography measurements for "normal" oceanic crust. Earth and Planetary Science Letters 499 (3), 145–156. https://doi.org/10.1016/j.epsl.2018.07.018.

Cruz, S.C.P., Alkmim, F.F., 2017. The Paramirim aulacogen. In: Heilbron, M., Cordani, U., Alkmim, F.F. (Eds.), São Francisco Craton, Eastern Brazil. Regional Geology Reviews. Springer, Switzerland, pp. 97–115. https://doi.org/10.1007/978-3-319-01715-0_6.

Cruz, S.C.P., Alkmim, F.F., Barbosa, J.S.F., Dussin, I., Gomes, L.C.C., 2015. Tectonic inversion of compressional structures in the southern portion of the Paramirim corridor, Bahia, Brazil. Braz. J. Genet. 45 (4), 541–567. https://doi.org/10.1590/2317-488920150030240.

Ernesto, M., 2005. Paleomagnetism of the Post-Palaeozoic alcaline magmatism in the Brazilian platform: questioning the mantle plume model. In: P, Gomes, C.B. (Eds.), Mesozoic to Cenozoic Alkaline Magmatism in the Brazilian Platform Comin-Chiaramonti. Edusp/Fapesp, São Paulo, pp. 689–705 200.

Ernst, R.E., Liikane, D.A., Jowitt, S.M., Buchan, K.L., Lanchar, J.A., 2019. A new plumbing system framework for mantle plume-related continental Large Igneous Provinces and their mafic-ultramafic intrusions. J. Volcanol. Geoth. Res. 384, 75–84 Doi.org/10.1016/j.jvolgeores.2019.07.007.
Ferrari, A., Riccomini, C., 1999. Campo de esforc¸os PlioPleistocenico na Ilha de Trindade (Oceano Atlântico Sul, Brasil) e sua relacão com a tectônica regional. Rev. Bras. Geociencias 29 (2), 195–202.
Ferreira, T.S., De Araújo, M.N.C., Da Silva, F.C.A., 2014. Cenozoic folding in the Cumuruxatiba basin, Brazil: an approach to the deformation trigger by the Abrolhos magmatism. Mar. Petrol. Geol. 54, 47–64. https://doi.org/10.1016/j.marpetgeo.2014.02.012.
Fodor, R., Mukasa, S.B., Gomes, C.B., Cordani, U.G., 1989. Ti-rich Eocene basaltic rocks, Abrolhos Platform, offshore Brazil, 18 S: petrology with respect to South Atlantic magmatism. J. Petrol. 30 (3), 763–786.
Forni, F., Degruyter, W., Bachmann, O., De Astis, G., Mollo, S., 2018. Long-term magmatic evolution reveals the beginning of a new caldera cycle at Campi Flegrei. Sci. Adv. 4 (11), 1–11. https://doi.org/10.1126/sciadv.aat9401.
Fossen, H., Cavalcante, G.C., de Almeida, R.P., 2017. Hot versus cold orogenic behavior: comparing the Araçuaí-west Congo and the Caledonian orogens. Tectonics 36, 2159–2178. https://doi.org/10.1002/2017TC004743.
Foulger, G.R., Natland, J.H., 2003. Is "hotspot" volcanism a consequence of plate tectonics?. Science 300, 921–922.
Franke, D., 2013. Rifting, lithosphere breakup and volcanism: comparison of magma-poor and volcanic rifted margins. Mar. Petrol. Geol. 43, 63–87.
França, R.L., Del Rey, A.C., Tagliari, C.V., Brandão, J.R., Fontanelli, P.D.R., 2007. Bacia do Espírito Santo. Bol. Geociencias Petrobras 15 (2), 501–509.
Gibson, S.A., Thompson, R.N., Leonardo, O.H., Dickin, A.P., Mitchel, J.G., 1995. The Late Cretaceous impact of the Trindade mantle plume: evidence from large-volume, mafic, potassic magmatism in SE Brazil. J. Petrol. 36 (1), 189–229.
Gomes, N.S., Suita, M.T.F., 2010. Ocorrência de vulcanismo bimodal de idade Terciaria na Bacia de Mucuri. Bol. Geociencias Petrobras 18 (2), 232–248.
Hansen, D.M., 2006. The morphology of intrusion-related vent structures and their implications for constraining the timing of intrusive events along the NE Atlantic margin. J. Geol. Soc. 163 (5), 789–800. https://doi.org/10.1144/0016-76492004-167.
Hansen, M., D., Redfern, J., Federici, F., di Biase, D., Bertozzi, G., 2008. Miocene igneous activity in the northern Subbasin, offshore Senegal, NW Africa. Mar. Petrol. Geol. 25, 1–15. https://doi.org/10.1016/j.marpetgeo.2007.04.007.
Hartnady, C.J.H., Le Roex, A.P., 1985. Southern Ocean hot spot tracks and the Cenozoic absolute motion of the African, Antarctic and South American plates. Earth Planet Sci. Lett. 75, 245–257.
Hasui, Y., Oliveira, M.A.F., 1984. Província Mantiqueira - setor central. Geociências 308–344.
Heilbron, M., Mohriak, W., Valeriano, C.M., Milani, E., Almeida, J.C.H., Tupinambá, M., 2000. From collision to extension: the roots of the south-eastern continental margin of Brazil. In: Talwani, Mohriak (Eds.), Atlantic Rifts and Continental Margins. American Geophysical Union, Geophysical Monograph Series, vol. 115. pp. 1–34.
Heilbron, M., Valeriano, C.M., Tassinari, C.C.G., Almeida, J., Tupinamba, M., Siga, O., Trouw, R., 2008. Correlation of Neoproterozoic terranes between the Ribeira Belt, SE Brazil and its African counterpart: comparative tectonic evolution and open questions. Geological Society, London, Special Publications 294, 211–237 Doi.org/10.2113/gselements.7.4.253.
Heine, C., Zoethout, J., Müller, R.D., 2013. Kinematics of South Atlantic rift. Solid Earth 4, 215–253 Doi.org/10.5194/se-4-215-2013.
Herz, N., 1977. Timing of spreading in the South Atlantic: information from Brazilian alkalic rocks. Geol. Soc. Am. Bull. 88, 101–112.
Jerram, D.A., Bryan, S.E., 2015. Plumbing systems of shallow level intrusive complexes. In: Breitkreuz, C., Rocchi, S. (Eds.), Physical Geology of Shallow Magmatic Systems. Advances in Volcanology (An Official Book Series of the International Association of Volcanology and Chemistry of the Earth's Interior). Springer, Cham. https://doi.org/10.1007/11157_2015_8.
Jourdan, F., Féraud, G., Bertrand, H., Watkeys, M.K., Kampunzu, A.B., Le Gall, B., 2006. Basement control on dyke distribution in Large Igneous Provinces: case study of the Karoo triple junction. Earth Planet Sci. Lett. 241 (1), 307–322.
Konrad, K., Graham, D.W., Kent, A.J.R., Koppers, A.P., 2018. Spatial and temporal variability in Marquesas Islands volcanism revealed by 3He/4He and the composition of olivine-hosted melt inclusions. Chem. Geol. Volume 477, 161–176 Doi.org/10.1016/j.chemgeo.2017.12.025.
Leat, P.T., 2008. On the long-distance transport of Ferrar magmas. In: Thomson, K., Petford, N. (Eds.), Structure and Emplacement of High-Level Magmatic Systems, vol. 302. Geological Society of London Special Publication, pp. 45–61 Doi.org/10.1144/SP302.4.
Magee, et al., 2019. Magma plumbing systems: a geophysical perspective. J. Petrol. 59 (No. 6), 1217–1251. https://doi.org/10.1093/petrology/egy064.
Magee, C., Briggs, F., Jackson, C.A.-L., 2013. Lithological controls on igneous intrusion-induced ground deformation. J. Geol. Soc. 170, 853–856.
Matthews, K.J., Maloney, K.T., Zahirovic, S., Williams, S.E., Seton, M., Müller, R.D., 2016. Global plate boundary evolution and kinematics since the late Paleozoic. Global Planet. Change. https://doi.org/10.1016/j.gloplacha.2016.10.002.
Mazza, S.E., Gazel, E., Johnson, E.A., Bizimis, M., McAleer, R., Biryol, C.B., 2017. Post-rift magmatic evolution of the eastern North American "passive-aggressive" margin. G-cubed 18, 3–22. https://doi.org/10.1002/2016GC006646.
Miller, H.G., Singh, V., 1994. Semiquantitative techniques for the removal of directional trends from potential field data. J. Appl. Geophys. 32, 213–217 Doi.org/10.1016/0926-9851(94)90022-1.
Miller, M.S., O'Driscoll, L.J., Butcher, A.J., Thomas, C., 2015. Imaging Canary Island hotspot material beneath the lithosphere of Morocco and southern Spain. Earth Planet Sci. Lett. 431, 186–194 Doi.org/10.1016/j.epsl.2015.09.026.
Mitchell, N.C., 2001. Transition from circular to stellate forms of submarine volcanoes. J. Geophys. Res. 106 (B2), 1987–2003. https://doi.org/10.1029/2000JB900263.
Mizusaki, A.M., Alves, D.B., Conceição, J.C.J., 1994. Eventos magmáticos nas bacias do Espirito Santo, Mucuri e Cumuruxatiba. In: CONGR. BRAS. GEOL. 38, Baln. Camboriú, B. Res. Expandidos. Baln. Camboriú: SBG L.. pp. 566–567.
Mohriak, W.U., 2005. Interpretação geológica e geofísica da Bacia do Espírito Santo e da região de Abrolhos: petrografia, datação radiométrica e visualização sísmica das rochas vulcânicas. Bol. Geociencias Petrobras 14, 133–142.
Mohriak, W.U., Rosendahl, B.R., Turner, J.P., Valente, S.C., 2002. Crustal architecture of South Atlantic volcanic margins. In: Menzies, M.A., Klemperer, S.L., Ebinger, C.J., Baker, J. (Eds.), Volcanic Rifted Margins: Boulder, Colorado, vol. 362. Geological Society of America Special Paper, pp. 159–202.
Montes-Lauar, C.R., 1993. Paleomagnetismo de rochas magmáticas mesozóico-cenozóicas da Plataforma Sul-Americana. (São Paulo).
Moreau, C., Demaiffe, D., Bellion, Y., Boullier, A.-M., 1994. A tectonic model for the location of Paleozoic ring complexes in Aïr (Niger, West Africa). Tectonophysics 234, 129–146.
Morgan, W.J., 1983. Hotspot tracks and the early rifting of the Atlantic. In: Morgan, P., Baker, B.H. (Eds.), Processes of Continental Rifting. Tectonophysics, vol. 94. pp. 123–139. https://doi.org/10.1016/B978-0-444-42198-2.50015-8.
Motoki, A., Novais, L.C.C., Motoki, K.F., De Oliveira, L.C., De Souza Fasolo, R., Lima, A.B., 2014. Satellite-derived gravimetry for Abrolhos continental shelf, States of Espírito Santo and Bahia, Brazil, and its relation to tectonic genesis of sedimentary basins. Rev. Bras. Geofís. 32 (4), 735–751.
Moulin, M., Aslanian, D., Unternehr, P., 2010. A new starting point for the south and equatorial Atlantic ocean. Earth Sci. Rev. 98, 1–37.
Muirhead, J.D., Airoldi, G., White, J.D., Rowland, J.V., 2014. Cracking the lid: sill-fed dikes are the likely feeders of flood basalt eruptions. Earth Planet Sci. Lett. 406, 187–197. https://doi.org/10.1016/j.epsl.2014.08.036.
Novais, L.C.C., Zelenka, T., Szatmari, P., Motoki, A., Aires, J.R., Tagliari, C.V., 2008. Ocorrência de rochas vulcânicas ignimbríticas na porção norte da Bacia do Espírito Santo: evolução do modelo tectono-sedimentar. Bol. Geociencias Petrobras 16 (1), 139–156.
O'Connor, J.M., Duncan, R.A., 1990. Evolution of the Walvis Ridge-Rio Grande rise hot spot system: implications for African and south American plate motions over plumes. J. Geophys. Res. 95 (B11), 17475–17502. https://doi.org/10.1029/JB095iB11p17475.
Oliveira, L.C., Novais, L.C.C., Motoki, A., Brito Neves, B.B., Borges Filho, R., Alves, D.B., Oliveira, R.P., Gama, R.M.A., Fasolo, R.S., Rocha, T.P., 2012. Nova ocorrência de riolito piroclástico na falésia da Praia de Costa Dourada, Mucuri, BA. Anais 46 Congresso Brasileiro de Geologia.
Oliveira, L.C., de Oliveira, R.M.A.G., Pereira, E., 2018. Seismic characteristics of the onshore Abrolhos magmatism, East-Brazilian continental margin. Mar. Petrol. Geol. 89, 488–499.
Pedrosa-Soares, A.C., Noce, C.M., Wiedeman, C.M., Pinto, C.P., 2001. The Araçuaí-West-Congo Orogen in Brazil: an overview of a confined orogen formed during Gondwanaland assembly. Precambrian Res. 110 (1–4), 307–323.
Oreiro, S.G., Cupertino, J.A., Szatmari, P., Thomas-Filho, A., 2008. Influence of pre-salt alignments in post-Aptian magmatism in the Cabo Frio high and its surroundings, Santos and Campos basins, SE Brazil: An example of non-plume-related magmatism. Journal of South American Earth Sciences 25 (1), 116–131.
Pedrosa-Soares, A.C., Alkmim, F.F., Tack, L., Noce, C.M., Babinski, M., Silva, L.C., Martins-Neto, M.A., 2008. Similarities and differences between the Brazilian and African counterparts of the neoproterozoic Araçuaí-west Congo orogen. Geological Society, London, Special Publications 294, 153–172.
Pinel, V., Jaupart, C., 2004. Likelihood of basaltic eruptions as a function of volatile content and volcanic edifice size. J. Volcanol. Geoth. Res. 137 (1), 201–217.
Pires, G.L.C., Bongiolo, E.M., Geraldes, M.C., Renac, C., Santos, A.C., Jourdan, F., Neumann, R., 2016. New 40Ar/39Ar ages and revised 40K/40Ar* data from nephelinitic–phonolitic volcanic successions of the Trindade Island (South Atlantic Ocean). J. Volcanol. Geoth. Res. 327, 531–538.
Planke, S., Rasmussen, T., Rey, S.S., Myklebust, R., 2005. Seismic characteristics and distribution of volcanic intrusions and hydrothermal vent complexes in the Vøring and Møre basins. In: Doré, A.G., Vining, B.A. (Eds.), Petroleum Geology: North-West Europe and Global Perspectives—Proceedings of the 6th Petroleum Geology Conference. pp. 833–844.
Rabinowitz, D., P., LaBrecque, J., 1979. The mesozoic South Atlantic ocean and evolution of its continental margin. Journal of Geophysical Research, Solid Earth 84, 5973–6002. https://doi.org/https://.org/10.1029/JB084iB11p05973.
Santos, A.C., Mohriak, W.U., Geraldes, M.C., Santos, W.H., Ponte-Neto, C.F., Stanton, N., 2018. Compiled potential field data and seismic surveys across the Eastern Brazilian continental margin integrated with new magnetometric profiles and stratigraphic configuration for Trindade Island, South Atlantic, Brazil. Int. Geol. Rev. 61 (14), 1728–1744. https://doi.org/10.1080/00206814.2018.1542634.
Schofield, N., Holford, S., Millett, J., Brown, D., Jolley, D., Passey, S.R., Muirhead, D., Grove, C., Magee, C., Murray, J., Hole, M., Jackson, C.A.-L., Stevenson, C., 2017a. Regional magma plumbing and emplacement mechanisms of the Faroe-Shetland Sill Complex: implications for magma transport and petroleum systems within sedimentary basins. Basin Res. 29, 41–63. https://doi.org/10.1111/bre.12164.
Schofield, N., Holford, S., Millett, J., Brown, D., Jolley, D., Passey, S., Muirhead, D., Grove, C., Magee, C., Murray, J., Hole, M., Jackson, C., Stevenson, C., 2017b. Regional Magma Plumbing and emplacement mechanisms of the Faroe-Shetland Sill Complex: implications for magma transport and petroleum systems within sedimentary basins. Basin Res. 29, 41–63.
Sengör, A.C., Burke, K., 1978. Relative timing of rifting and volcanism on Earth and its tectonic implications. Geophys. Res. Lett. 5 (6), 419–421.

Siebel, W., Becchio, R., Volker, F., Hansen, M.A.F., Viramonte, J., Trumbull, R.B., Haase, G., Zimmer, M., 2000. Trindade and Martín Vaz islands, South Atlantic: isotopic (Sr, Nd, Pb) and trace element constraints on plume related magmatism. J. S. Am. Earth Sci. 13, 79–103.

Sobreira, J.F.F., França, R.L., 2006. Um modelo tectono-magmático para a região do complexo vulcânico de Abrolhos. Bol. Geociencias Petrobras 14, 143–147.

Sobreira, J.F.F., Szatmari, P., 2003. Idades Ar–Ar para as rochas ıgneas do Arquipélago de Abrolhos, margem sul da Bahia. In: IX SNET–Simpósio Nacional de Estudos Tectônicos, Abstracts. pp. 382–383.

Stanton, N., Manatschal, G., Autin, J., Sauter, D., Maia, M., Viana, A., 2016. Geophysical fingerprints of hyper-extended, exhumed and embryonic oceanic domains: the example from the Iberia–Newfoundland rifted margins. Mar. Geophys. Res. 37, 185. https://doi.org/10.1007/s11001-016-9277-0.

Svensen, H., Planke, S., Malthe-Sorenssen, A., Jamtveit, B., Myklebust, R., Rasmussen Eidem, T., Rey, S.S., 2004. Release of methane from a volcanic basin as a mechanism for initial Eocene global warming. Nature 429, 542–545 6991 https://doi.org/10.1038/nature02566.Talwani.

Svensen, H., Jamtveit, B.Ø., Planke, S., Chevallier, L., 2006. Structure and evolution of hydrothermal vent complexes in the Karoo Basin. South Africa J. Geol. Soc. 163 (4), 671–682.

Tack, L., Wingate, M.T.D., Liégois, J.-P., Fernandez-Alonso, M., Deblond, A., 2001. Early neoproterozoic magmatism (1000–910 Ma) of the Zadinian and Mayumbian groups (Bas-Congo): onset of Rodinia rifting at the western edge of the Congo craton. Precambrian Res. 110 (1–4), 277–306. https://doi.org/10.1016/S0301-9268(01)00192-9.

Talwani, M., Worzel, J.L., Landisman, M., 1959. Rapid gravity computations for two-dimensional bodies with application to the mendocine submarine fracture zone. J. Geophys. Res. 64, 49–61.

Thompson, R.N., Gibson, S.A., Mitchell, J.G., Dickin, A.P., Leonardos, O.H., Brod, J.A., J, C., 1998. Greenwood, migrating cretaceous–eocene magmatismin the Serra do mar alkaline province,SE Brazil: melts from the deflected trindade mantle plume?. J. Petrol. 39 (8), 1493–1526. https://doi.org/10.1093/petroj/39.8.1493.

Thouret, J.C., 1999. Volcanic geomorphology - an overview. Earth Sci. Rev. 47 (1–2), 95–131. https://doi.org/10.1016/S0012-8252(99)00014-8.

Torsvik, T.H., Rousse, S., Labails, C., Smethurst, M.A., 2009. A new scheme for the opening of the south Atlantic ocean and dissection of an Aptian salt basin. Geophys. J. Int. 177, 1315–1333.

Trompette, R., 1994. Geology of Western Gondwana (2000–500 Ma), PanAfricanBrasiliano Aggregation of South America and Africa. Balkema Press, Rotterdam, Rotterdam.

Van Den Bogaard, P., 2013. The origin of the Canary Island Seamount Province-New ages of old seamounts. Sci. Rep. 3, 2107.

Vauchez, A., Egydio-Silva, M., Babinski, M., Tommasi, A., Uhlein, A., Liu, D., 2007. Deformation of a pervasively molten middle crust: insights from the neoproterozoic Ribeira-Araçuaí orogen (SE Brazil). Terra. Nova 19, 278–286 Doi.org/10.1111/j.1365-3121.2007.00747.x.

Vincentelli, M.G.C., Mirna Neves, M., Morales, N., 2016. Controle estrutural do Neógeno e Quaternário nas bacias de Campos e do Espírito Santo. Geociencias 35 (1), 47–62.

White, R., McKenzie, D., 1989. Magmatism at rift zones: the generation of volcanic continental margins and flood basalts. J. Geophys. Res. 94 (B6), 7685–7729. https://doi.org/10.1029/JB094iB06p07685.

Worzel, M., J, L., Landisman, M., 1959. Rapid gravity computations for two-dimensional bodies with application to the Mendocino submarine fracture zone. J. Geophys. Res. 64 (1), 49–59. https://doi.org/10.1029/JZ064i001p00049.